nature chemical biology

ARTICLES

https://doi.org/10.1038/s41589-020-00702-5

Check for updates

Conformational rearrangement during activation of a metabotropic glutamate receptor

Brandon Wey-Hung Liauw[1,2], Hamid Samareh Afsari[1,2] and Reza Vafabakhsh[1]✉

G protein-coupled receptors (GPCRs) relay information across cell membranes through conformational coupling between the ligand-binding domain and cytoplasmic signaling domain. In dimeric class C GPCRs, the mechanism of this process, which involves propagation of local ligand-induced conformational changes over 12 nm through three distinct structural domains, is unknown. Here, we used single-molecule FRET and live-cell imaging and found that metabotropic glutamate receptor 2 (mGluR2) interconverts between four conformational states, two of which were previously unknown, and activation proceeds through the conformational selection mechanism. Furthermore, the conformation of the ligand-binding domains and downstream domains are weakly coupled. We show that the intermediate states act as conformational checkpoints for activation and control allosteric modulation of signaling. Our results demonstrate a mechanism for activation of mGluRs where ligand binding controls the proximity of signaling domains, analogous to some receptor kinases. This design principle may be generalizable to other biological allosteric sensors.

Cells use membrane receptors to dynamically sense and interpret chemical and physical signals from their environment[1]. A key design principle of many membrane receptors is that sensing is energetically passive, and no external energy is required. That is, the energetics of ligand binding is converted to a local conformational change and into the output signal. This process is often allosteric in nature and involves coupling of conformational dynamics between the ligand-binding 'sensory domain' and the cytoplasmic 'signaling interface'[2].

In humans, G protein-coupled receptors (GPCRs) are the largest family of membrane receptors and have become key targets for drug development due to their involvement in nearly all physiological processes[3,4]. A deeper understanding of the activation and modulatory mechanisms used by GPCRs would be critical for developing new therapeutics, as well as designing synthetic receptors and sensors. Major advances in structural methods have lead to identification of ligand- and ion-binding sites in many GPCRs[3,5], as well as atomic-level details of different steps of signal transduction by GPCR complexes[6,7]. Moreover, improved understanding of the conformational dynamics of GPCRs by computational, NMR spectroscopy, double electron–electron resonance spectroscopy and fluorescent-based assays have demonstrated that the two-state on–off model of GPCRs cannot account for their signaling versatility and complex pharmacology, and GPCRs are highly dynamic proteins that sample multiple conformational states[8–11]. Collectively, these approaches have started to provide a structural framework to understand multiple facets of GPCR pharmacology, such as basal activity, partial agonism, biased signaling and allosteric modulation[7,12–14]. However, how large-scale conformational changes propagate during the activation process of GPCRs, and how ligands modify the structure and dynamics of GPCRs to tune their functional outcomes, especially for many large multidomain GPCRs, are poorly understood.

Among all GPCRs, class C GPCRs are structurally unique in that they have multiple structural domains and function as obligate dimers. Importantly, they have a large extracellular domain that contains the ligand-binding pocket. Metabotropic glutamate receptors (mGluRs) are class C GPCRs that are responsible for the slow neuromodulatory effects of glutamate and are essential for tuning synaptic transmission and excitability[15,16]. Structural[17–19] and spectroscopic studies[20,21] have shown that unlike the activation process of most class A GPCRs, which is associated with subtle motions in the extracellular domain of the receptor, the activation of mGluRs involves local and global conformational changes that propagate through the three structural domains of the receptor, over 12 nm, to reach the intracellular G protein-binding interface (signaling interface)[10,17,21] (Fig. 1a). The molecular details, timescales, intermediate transition states and sequence of conformational changes during this process are unclear.

Here, we used single-molecule fluorescence resonance energy transfer (smFRET)[22] and in vivo FRET imaging to visualize the propagation of conformational changes during the activation of mGluR2. To circumvent limitations of common site-specific fluorescent labeling approaches that require generation of cysteine-less mutants or insertion of a large protein tag, we adopted and optimized an unnatural amino acid-incorporation strategy[23–25]. This enabled us to follow the conformation of the key allosteric linker between the ligand-binding and signaling domains of mGluR2. Using this assay, we found that the dimeric arrangement of mGluR2 adopts four distinct conformational states that are visited sequentially, in contrast to the two-state model deduced from the atomic structures[17,18]. Using mutations and cross-linking approaches, we characterized the functional property and importance of the conformational states for receptor signaling and modulation. This sequential four-state activation model provides a structural framework for understanding ligand efficacy and allosteric modulation of mGluRs and possibly other class C GPCRs.

Results

According to the current activation model for mGluRs, glutamate binding at the Venus flytrap (VFT) domain (sensory domain) closes the VFT lobes and results in the rearrangement of the dimer interface of the VFT domains from 'relaxed' to 'active'[10,18] (Fig. 1a). Next, this conformational change is thought to bring the adjacent

[1]Department of Molecular Biosciences, Northwestern University, Evanston, IL, USA. [2]These authors contributed equally: Brandon Wey-Hung Liauw, Hamid Samareh Afsari. ✉e-mail: reza.vafabakhsh@northwestern.edu

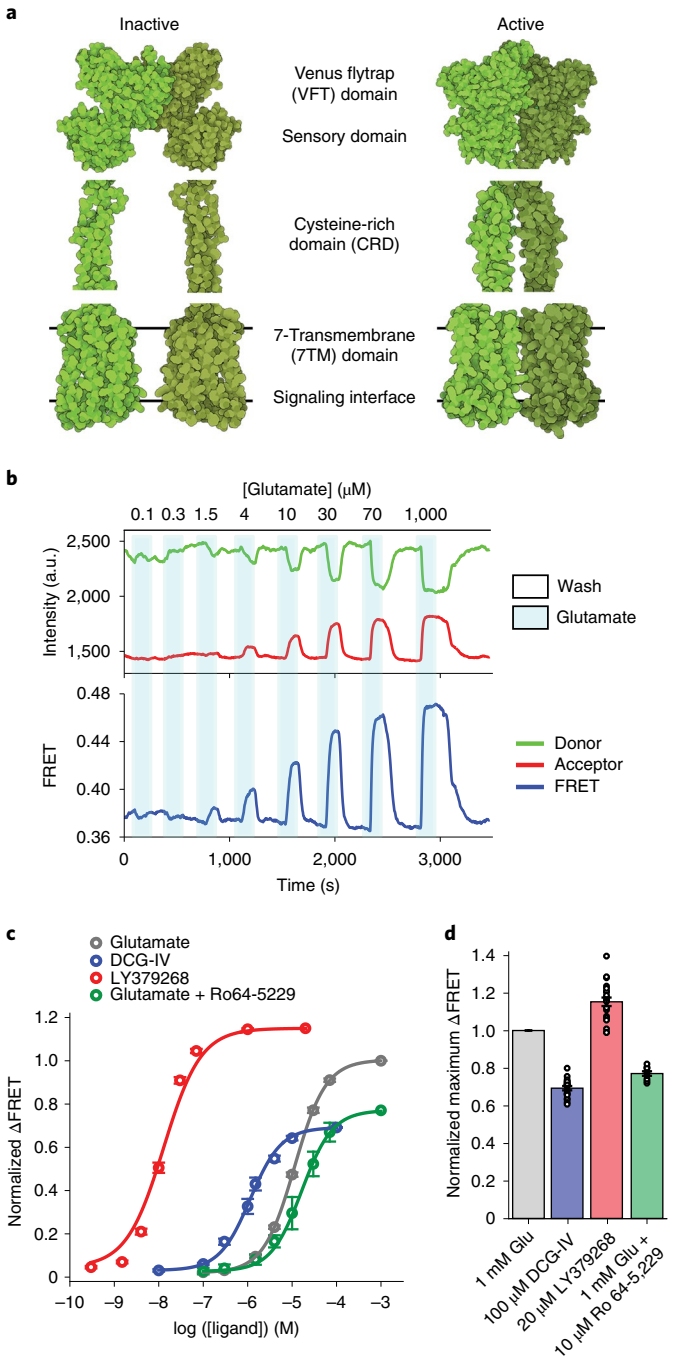

Fig. 1 | Characterization of the FRET-based CRD conformational sensor. **a**, Cartoon illustrating the arrangement of the three structural domains of mGluR5 in the inactive (PDB 6N52) and active (PDB 6N51) states. **b**, Representative donor and acceptor intensities and corresponding FRET signal from a cell in response to glutamate application. **c**, Dose–response curves from live-cell FRET titration experiments for glutamate (gray), LY379268 (red), DCG-IV (blue) or glutamate + 10 μM Ro64-5229 (green) in HEK293T cells. Each titration curve is normalized to the 1 mM glutamate response. Data represent mean ± s.e.m. of $N = 26$, 20, 10 and 13 cells for glutamate, LY379268, DCG-IV and glutamate + 10 μM Ro64-5229, respectively, examined over three independent experiments. **d**, Maximum FRET change in the presence of saturating LY379268 (red), DCG-IV (blue) and glutamate + 10 μM Ro64-5229 (green) normalized to the 1 mM glutamate response (gray) in HEK293T cells. Data represent mean ± s.e.m. of $N = 21$, 19 and 9 cells for LY379268, DCG-IV and glutamate + 10 μM Ro64-5229, respectively, examined over three independent experiments.

cysteine-rich domains (CRDs) closer together to activate the G protein-binding interface[17,21] (Fig. 1a). The CRD is the allosteric structural link that relays the incoming signal (that is, the conformation of the VFT domains) to the signaling site in the seven-helix transmembrane (7TM) domains (Fig. 1a). We therefore hypothesized that the arrangement of the CRDs in the dimer reports how the VFT domains allosterically regulate the conformation of the 7TM domains, independent of intradomain movement of transmembrane helices. To test this, we applied smFRET and live-cell ensemble FRET imaging to visualize the conformational changes of the CRD of mGluR2 during activation, in real time[10,20,22].

Design and validation of CRD conformational FRET sensor. To attach donor and acceptor fluorophores site specifically, with minimal perturbation to the receptor structure, we adopted and optimized an unnatural amino acid-incorporation strategy[23–25] and introduced a 4-azido-L-phenylalanine at amino acid 548 of mouse mGluR2 (hereafter, 548UAA) (Extended Data Fig. 1a,b). We expressed 548UAA in HEK293T cells and labeled the cell-surface population of receptors with FRET donor (Cy3) and acceptor (Cy5) fluorophores site specifically, through a copper-catalyzed azide-alkyne click reacion[26] (Extended Data Fig. 1a,b and Methods). Because mGluRs are strict dimers, any FRET signal is exclusively from the receptors that are labeled with a single donor and a single acceptor fluorophore. Total cell lysate from labeled cells on a nonreducing polyacrylamide gel showed a single band corresponding to the size of the full-length dimeric mGluR2 (Extended Data Fig. 1c), verifying that the receptor population on the plasma membrane is full length.

We observed that glutamate induced a concentration-dependent increase in the FRET signal in labeled cells expressing 548UAA (Fig. 1b and Extended Data Fig. 1d), confirming a general decrease in the distance between the CRDs upon activation, and consistent with previous structural and cross-linking experiments[17,27,28]. This glutamate-dependent increase in ensemble FRET had a half-maximum effective concentration (EC_{50}) of 11.8 ± 0.5 μM (Fig. 1c), consistent with the concentration dependence of GIRK current activation in HEK293T cells[10]. Similar dose-dependent increase in the FRET efficiency was obtained with other orthosteric agonists LY379268 (hereafter, LY37) and DCG-IV with respective EC_{50} values of 12.8 ± 0.5 nM and 1.2 ± 0.2 μM (Fig. 1c and Extended Data Fig. 2a), matching the published range for mGluR2 (ref. [20]). On the other hand, the mGluR2-specific negative allosteric modulator (NAM) Ro64-5229 reduced the glutamate efficacy (maximum response 77% ± 1% of glutamate) (Fig. 1d) and potency (EC_{50} = 17.2 ± 1.1 μM) (Fig. 1c and Extended Data Fig. 2a), which is consistent with the notion that the CRD is the allosteric linker between ligand binding and signaling. Therefore, the 548UAA FRET sensor allows unperturbed quantitative analysis of ligand-induced conformational changes of the CRD in live cells. Importantly, the efficacy of ligands as characterized by signaling assays or VFT domain FRET sensors[10,20] correlates with the ligand-induced FRET change at the CRD, with DCG-IV being a partial agonist and LY37 > glutamate > DCG-IV (Fig. 1d and Extended Data Fig. 2b).

CRD is in dynamic equilibrium between four states. To perform smFRET imaging, cells expressing 548UAA with a C-terminal FLAG-tag were labeled with donor and acceptor fluorophores and then lysed. The cell lysate was applied onto a polyethylene glycol (PEG) passivated coverslip functionalized with anti-FLAG-tag antibody to immunopurify the receptors (SiMPull)[10,29] for total internal reflection fluorescence (TIRF) imaging (Extended Data Fig. 3a and Methods). In the absence of glutamate (inactive receptor), the CRD of individual mGluR2 receptors displayed rapid transitions between multiple FRET states (Fig. 2a and Extended Data Fig. 3b), in stark contrast to the previously reported behavior of the VFT domains, which were stable in a single conformation[10] (Extended

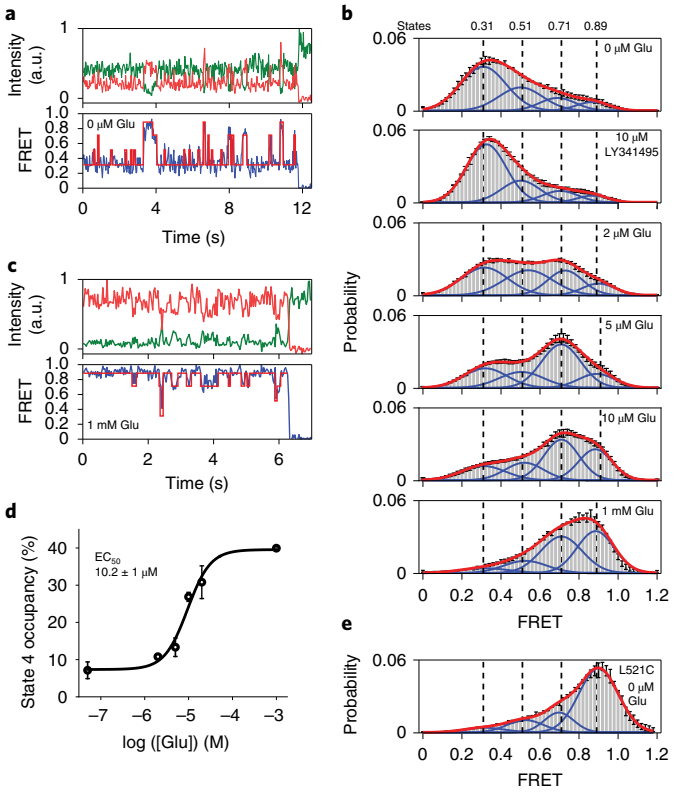

Fig. 2 | Single-molecule FRET reveals four conformational states of mGluR2 CRD. a, Example single-molecule time trace of 548UAA in the absence of glutamate showing donor (green) and acceptor (red) intensities. Corresponding FRET (blue) is overlaid with the predicted state sequence (red, bottom). **b**, smFRET population histograms in the presence of competitive antagonist (LY341495) and a range of glutamate concentrations. Data represent mean ± s.e.m. of $N = 3$ independent experiments. Total molecules examined for LY341495 and 0 μM, 2 μM, 5 μM, 10 μM and 1 mM glutamate conditions were 440, 250, 378, 879, 726 and 152, respectively. Histograms were fitted (red) to four Gaussian distributions (blue) centered around 0.31 (state 1), 0.51 (state 2), 0.71 (state 3) and 0.89 (state 4), denoted with dashed lines. **c**, Example single-molecule time trace of 548UAA in the presence of 1 mM glutamate showing donor (green) and acceptor (red) intensities. Corresponding FRET (blue) is overlaid with the predicted state sequence (red, bottom).
d, Glutamate dose–response curve of state 4 occupancy. State 4 occupancy is defined as the area of Gaussian distribution centered at 0.89 as a fraction of the total area. Data represent mean ± s.e.m. of $N = 3$ independent experiments. Total molecules examined as in **b** (216 total molecules for 20 μM glutamate). **e**, smFRET population histogram of the cross-linked constitutively active 548UAA (L521C; 176 total molecules) construct in the absence of glutamate. Data represent mean ± s.e.m. of $N = 3$ independent experiments. Four FRET states are denoted with dashed lines.

Data Fig. 3c). Histograms of smFRET data from many single receptors revealed four conformations with smFRET efficiency peaks at: 0.31, 0.51, 0.71 and 0.89 (labeled as states 1–4) (Fig. 2b, top histogram). The smFRET histogram was unchanged in the presence of saturating competitive antagonist LY341495 (Fig. 2b), confirming that the observed dynamics are independent of orthosteric agonist binding. In the presence of glutamate, receptors remained dynamic and showed transitions between the same four FRET states but with shifted occupancy to the higher states, in a glutamate-dependent manner (Fig. 2b and Extended Data Fig. 4a) and in qualitative agreement with the live-cell FRET experiment (Fig. 1b). Notably, even at saturating glutamate (1 mM), receptors showed substantial dynamics between states 3 and 4 (Fig. 2c and Extended Data Fig. 4b). A similar overall behavior was observed when examining mouse mGluR3 at the analogous position (A557) (Extended Data Fig. 5). The atomic structures of the inactive conformations of mGluR5 and mGluR3 have resolved the CRDs at a large distance apart (68.3 Å at position D560 in human mGluR5)[17,27]. Therefore, the lowest FRET peak at 0.31 (state 1), which is the predominant population in the absence of an agonist, corresponds to the crystallographic inactive conformation of mGluR2. In this conformation the VFT domain lobes are 'open' (oo) and the dimer interface is in the 'relaxed' (R) state (R/oo)[18,20]. On the other hand, the highest FRET peak at 0.89 (state 4) corresponds to an approximate distance of 38 Å, which agrees with the distance at our labeling position on the basis of the recent structure of the ligand-bound mGluR5 (ref. [17]) (35.9 Å at position D560 in human mGluR5). The occupancy of this FRET peak showed a glutamate concentration dependence with the EC_{50} value of 10.2 ± 1 μM (Fig. 2d) matching the EC_{50} value measured from signaling assays in live cells. Therefore, we hypothesized that the FRET state 4 is the crystallographic active CRD conformation of mGluR2. To test this, we performed a smFRET experiment on the intersubunit CRD cross-linked mGluR2(L521C) construct, which was previously shown to result in a constitutively signaling-active receptor[28]. Consistent with this, live-cell measurements with this construct showed no FRET change upon application of glutamate (Extended Data Fig. 6). smFRET experiments with this construct in the absence of glutamate showed a dominant peak at FRET 0.89 (Fig. 2e). Together, these results confirm the assignment of state 4 as the active CRD conformation of mGluR2.

In the presence of other mGluR2 orthosteric agonists, LY37 and DCG-IV, the CRD populated the same four FRET states (Fig. 3a and Extended Data Fig. 7a). Importantly, at saturating concentrations, LY37 showed 21% higher occupancy of the active-state conformation than glutamate, while DCG-IV showed 23% lower occupancy, which is consistent with their respective efficacy (Fig. 3b and Extended Data Fig. 7b). We further examined the nature and time ordering of transitions using a four-state hidden Markov model (HMM)[30,31]. The results of the HMM analysis as a transition density plot (TDP) at different glutamate concentrations demonstrate three distinct sets of bidirectional transitions between the four FRET states (Fig. 3c). Importantly, this analysis showed that transitions are sequential, happening between adjacent FRET peaks (0.31↔0.51↔0.71↔0.89). Together, these findings confirm the existence of four CRD conformations in the presence or absence of orthosteric agonists, and support a stepwise compaction of mGluR2 during activation, which is consistent with a conformational selection mechanism[32].

Conformations of CRDs and VFT domains are loosely coupled. Our observation that, in the presence of saturating full agonist (1 mM glutamate) or absence of ligand the CRD is dynamic (Fig. 2a,c and Extended Data Fig. 8), is in stark contrast with the behavior of the VFT domains of mGluR2, which adopt a distinct stable conformation in these conditions[10] (Extended Data Fig. 3c). Quantification of receptor dynamics using the cross-correlation of donor and acceptor signals also showed similar contrast between the dynamic behavior of the two adjacent domains (Fig. 3d). Consistent with the reduction of the dynamics of VFT domains in zero or saturating glutamate (1 mM), the amplitude of anticorrelation between donor and acceptor fluorophores for the VFT domain sensor (Extended Data Fig. 3c) vanished (Fig. 3d). However, the CRD sensor showed strong amplitude in both these conditions (Fig. 3d). Together, these results indicate that the conformation of the VFT domains and CRDs are allosterically loosely coupled. Such loose coupling was previously observed in molecular dynamics simulations and NMR experiments of β_2-adrenergic receptor (β_2AR)[33,34]. Our findings extend this notion to the multidomain class C GPCRs, suggesting

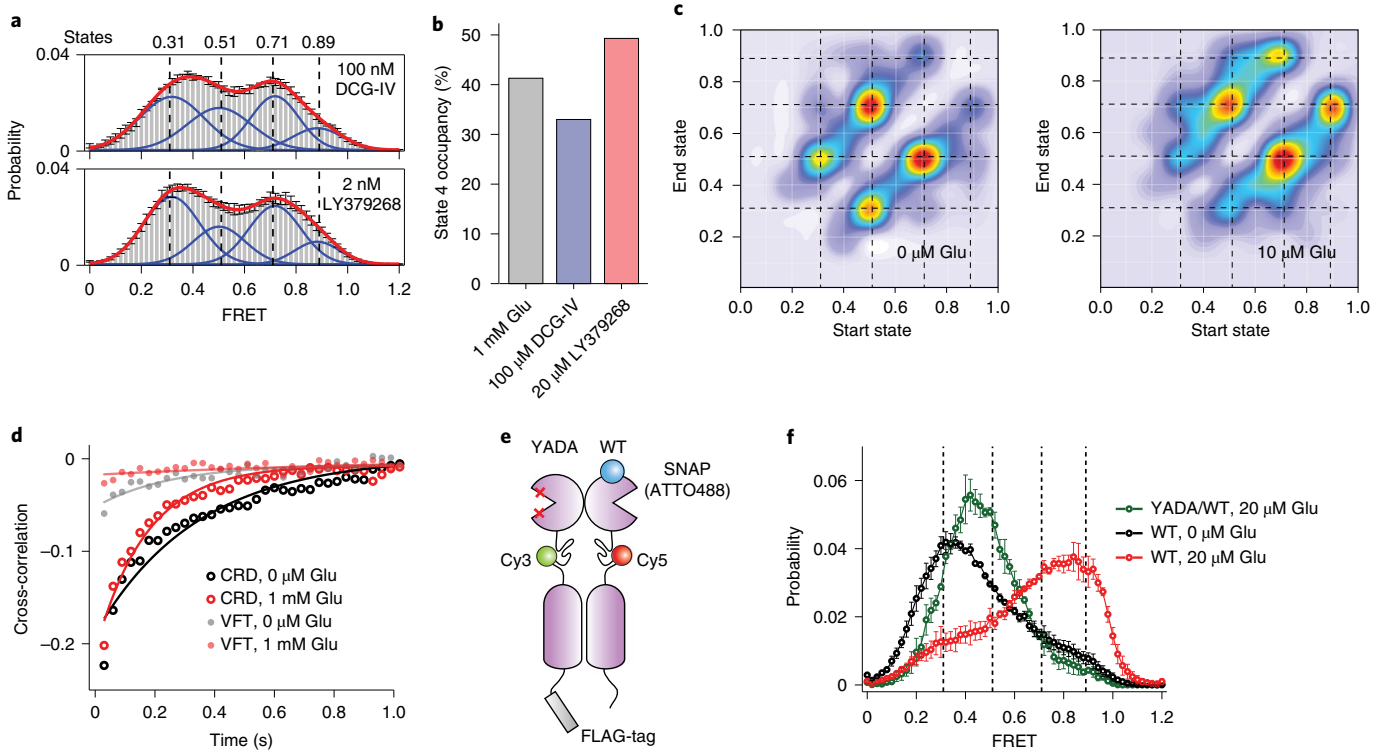

Fig. 3 | Activation of mGluR2 is a stepwise process. a, smFRET population histogram of 548UAA sensor in the presence of intermediate concentrations of orthosteric agonists DCG-IV (top; 166 total molecules) and LY379268 (bottom; 220 total molecules). Data represent mean ± s.e.m. of $N = 3$ independent experiments. Histograms are fitted (red) to four Gaussian distributions (blue) centered on 0.31 (state 1), 0.51 (state 2), 0.71 (state 3) and 0.89 (state 4), as denoted by dashed lines. **b**, State 4 (active state) occupancy at saturating concentrations of mGluR2 orthosteric agonists. State 4 occupancy is defined as the area of Gaussian distribution centered at 0.89 as a fraction of the total area. FRET peak fitting and area calculations were performed on average histograms. **c**, TDPs of 548UAA. Dashed lines represent four distinct FRET states. Transitions are from two independent measurements. **d**, Cross-correlation plots comparing the dynamics of the CRDs and VFT domains of mGluR2 at 0 and 1 mM glutamate. Data are from three independent measurements. Data were fitted to a single exponential decay function. **e**, Schematic of mGluR2 receptor constructs for the 548UAA YADA/WT heterodimer experiment. **f**, smFRET population histogram of 548UAA YADA/WT heterodimer in the presence of 20 μM glutamate (55 total molecules) compared to 548UAA WT (250 and 216 total molecules for 0 μM and 20uM glutamate). Data represent mean ± s.e.m. of $N = 3$ independent experiments. Dashed lines represent four distinct FRET states. Heterodimer data were acquired at 100 ms time resolution.

that loose allosteric coupling might be a more general feature of GPCRs and allosteric receptors as a whole, and is consistent with observations of distinct inter- and intradomain rearrangement timescales in mGluR1 (ref. [35]). Finally, the loose allosteric coupling that we uncovered here suggests that the CRD conformation, and not the VFT domain conformation, is the more accurate metric to report the activation of mGluRs, and perhaps class C GPCRs.

State 2 results from the closure of a single VFT domain. We further examined the correlation between the VFT domain lobe closure and the CRD conformation by performing smFRET experiments on receptors with a single glutamate-binding defective monomer[36] (548UAA YADA with Y216A and D295A mutations). This was achieved by co-expressing the C-terminal FLAG-tagged 548UAA YADA construct and an N-terminal SNAP-tagged 548UAA construct (Fig. 3e). Following the expression, the cell-surface population was labeled with BG-ATTO488 (SNAP-tag substrate) as well as Cy3 and Cy5 as before (see Methods). Particles that were pulled down with the anti-FLAG antibody and showed the ATTO488 signal plus FRET donor and acceptor signals were analyzed. smFRET analysis showed that at 20 μM glutamate the CRD of the YADA/wild type (WT) heterodimer predominantly occupies state 2 (Fig. 3f and Extended Data Fig. 9) with brief visits to higher FRET states, supporting the assignment of state 2 to a configuration in which one VFT domain is 'closed' and the other is 'open' (co) with the VFT domain interface in the 'relaxed' (R) form and the receptor in the inactive state (R/co).

State 3 represents a pre-active receptor conformation. To investigate the identity of state 3 in mGluR2 activation we quantified the occupancy of all four states as a function of increasing glutamate (Fig. 4a). While the occupancy of the active state 4 continuously increased with increasing glutamate concentration, state 3 occupancy initially increased and then plateaued around the EC_{50} concentration of glutamate. This observation, and the fact that in saturating agonist the VFT domains are locked in a single active (A/cc) conformation (Extended Data Fig. 3c), while the CRDs dynamically transition mostly between states 3 and 4 (Fig. 2b,c and Extended Data Fig. 8), suggest that state 3 represents a pre-active conformation of the receptor. In this conformation the VFT domains are in the active arrangement (A/cc)[10], yet the receptor is inactive. Existence of such a pre-active state could be the consequence of a rate-limiting step during the activation process, such as intrasubunit conformational changes that contribute to formation of the active receptor. This interpretation is consistent with recent experiments that showed that activation of mGluR1 involves a fast and a slow time constant[35]. Finally, cross-linking and structural studies have shown that in the active state of mGluRs, the 7TM domains interact along the TM6 helix[17,37]. Thus, it is likely that the pre-active state 3 is a conformation

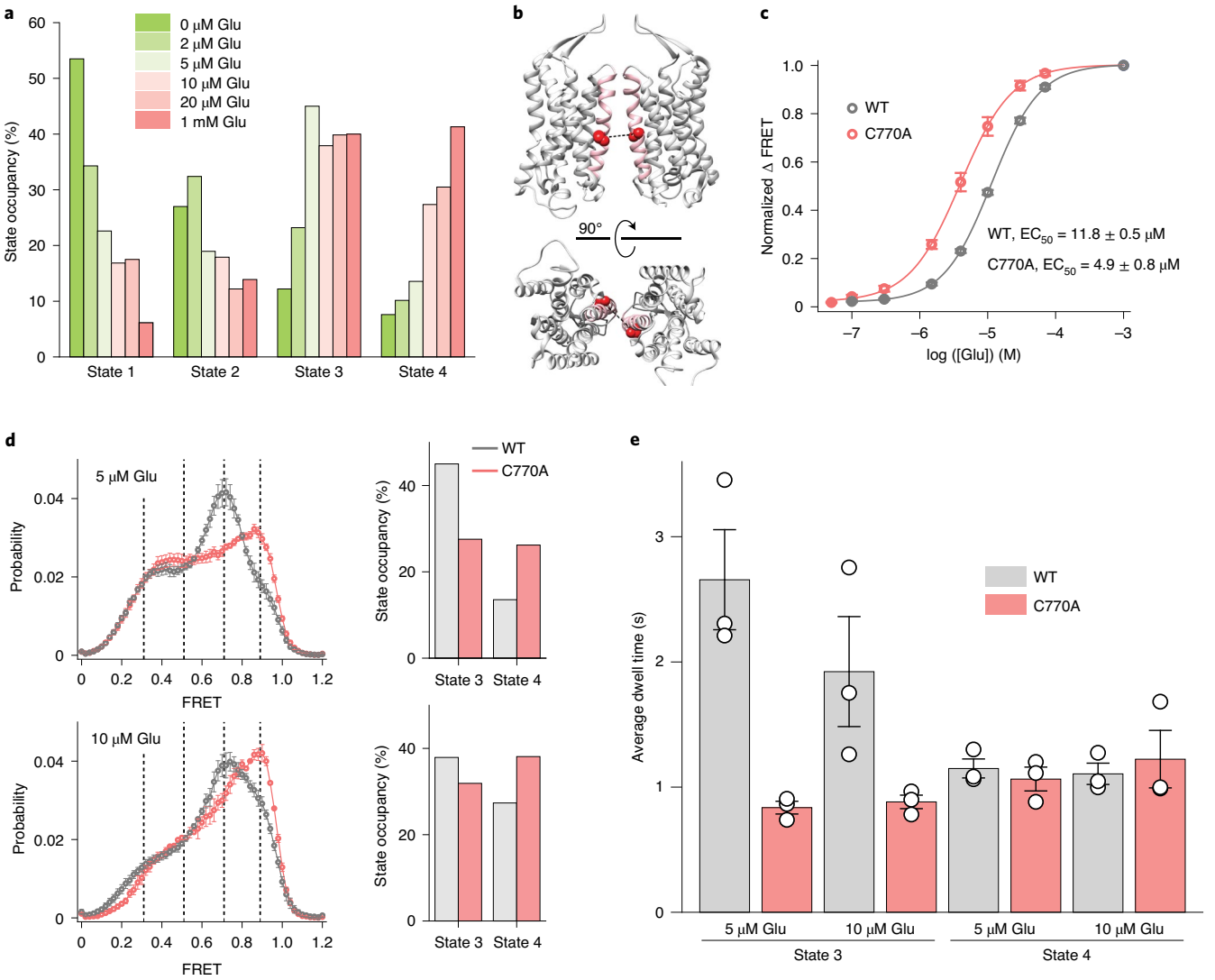

Fig. 4 | Conformational state 3 is a pre-active conformation of mGluR2. a, Occupancy of the four conformational states of the CRD in the presence of increasing glutamate concentrations. Values represent area under each FRET peak from smFRET population histograms, centered at 0.31 (state 1), 0.51 (state 2), 0.71 (state 3) and 0.89 (state 4) and as the fraction of the total area. **b**, The PAM mutation (C770A, red spheres) on the structure of mGluR5 (PDB 6N51). TM6 is colored in pink. **c**, Dose–response curves from live-cell FRET glutamate titration experiments for the 548UAA WT and C770A PAM receptor. Each curve is normalized to the 1 mM glutamate response. Data represent mean ± s.e.m. of $N = 26$ and 13 cells expressing 548UAA WT or C770A PAM receptors, respectively, examined over three independent experiments. **d**, smFRET population histograms of 548UAA WT receptors (gray) at 5 μM (879 total molecules) and 10 μM glutamate (726 total molecules) and C770A PAM receptors (red) at 5 μM (689 total molecules) and 10 μM glutamate (370 total molecules). Data represent mean ± s.e.m. of $N = 3$ independent experiments. Dashed lines represent the four FRET states. Bar graphs represent area of FRET state 3 (FRET = 0.71) and state 4 (FRET = 0.89) as the fraction of total area for WT and PAM mutant receptor. **e**, Dwell times of states 3 and 4 for the WT receptor at 5 μM (147 total molecules) and 10 μM glutamate (140 total molecules) and PAM mutant receptor at 5 μM (128 total molecules) and 10 μM glutamate (142 total molecules). Average dwell time was calculated by fitting a single exponential decay function to dwell-time histograms for each condition. Dwell times represent mean ± s.e.m. of $N = 3$ independent experiments at 100 ms. FRET peak fitting and area calculations were performed on averaged histograms.

in which the 7TM domains are brought into close proximity through the VFT domain closure (A/cc conformation of the VFT domains) yet have not adopted the signaling-competent configuration of the 7TM domain. Consistent with this interpretation is that the active state 4 is transient (Fig. 2c and Extended Data Fig. 4).

To investigate the importance of the pre-active state 3 for receptor signaling, we studied the conformational dynamics of mGluR2 containing the mutation C770A (Fig. 4b). This mutation is shown to enhance mGluR signaling in a manner similar to a positive allosteric modulator (PAM)[20,38]. Live-cell ensemble experiments for 548UAA with this PAM mutation showed increased mGluR2 sensitivity to glutamate ($EC_{50} = 4.9 \pm 0.8$ μM compared to 11.8 ± 0.5 μM for the WT receptor), suggesting that the PAM effect of this mutation in the 7TM domain is allosterically detectable at the CRD (Fig. 4c). We next performed smFRET analysis of this construct and observed the same four states as the wild-type receptor (Extended Data Fig. 10a). However, at each glutamate concentration tested, the occupancy of the active state (state 4) was increased for the mutant compared to the wild-type receptor (Fig. 4d), consistent with the expected response from a PAM and further confirming that the immobilized receptors retain functional properties of the 7TM domain. To test whether this effect is due to increased lifetime of the active state or increased visits to the active state, we performed dwell-time analysis of states 3 and 4 with the PAM construct. Remarkably, while the lifetime of active

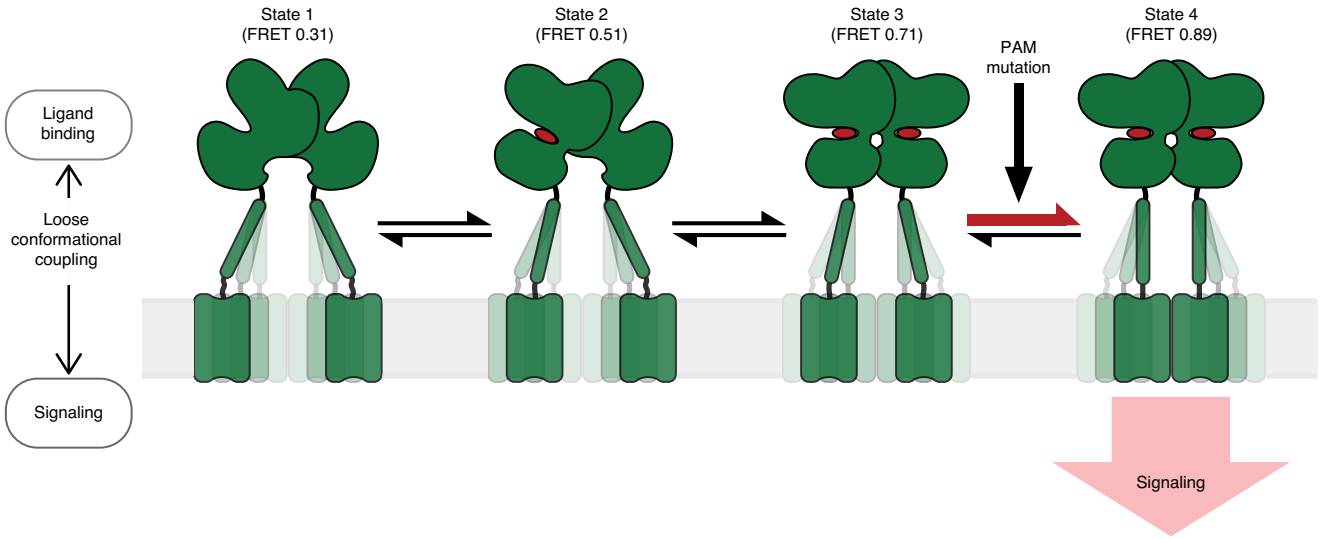

Fig. 5 | Schematic of the stepwise activation model for mGluR2. Four-state stepwise model for the mechanism of allosteric activation of mGluRs, with receptors shown in green and ligand in red. Darker shading of CRDs and 7TM domains represents greater occupancy of a given conformation. State 1 (FRET = 0.31) represents the most common CRD conformation of an unliganded receptor, where the CRDs are farthest apart. State 2 (FRET = 0.51) represents the CRD conformation resulting from ligand binding to a single VFT domain. State 3 (FRET = 0.71) represents the CRD conformation resulting from ligand binding to both VFT domains and before the formation of a stabilizing 7TM domain interaction. State 4 (FRET = 0.89) represents the CRD conformation resulting from ligand binding to both VFT domains and a stabilizing 7TM domain interaction. State 4 is the active conformation of the receptor. PAM mutations can function by increasing transitions from state 3 to 4.

state 4 was similar between WT and the PAM mutant, the lifetime of state 3 was reduced about threefold for the PAM mutant (Fig. 4e and Extended Data Fig. 10b). TDP analysis revealed that there were more transitions from state 3 to state 4 for the PAM mutant compared to WT (Extended Data Fig. 10c). Considering that only state 3 exhibits a substantially altered lifetime for the PAM mutant, while the lifetimes of the other states remain mostly unchanged (Extended Data Fig. 10d), and the fact that the major FRET histogram population change is the shift from state 3 to state 4 occupancy, our results show that the C770A PAM mutation confers its modulatory effect allosterically by increasing transitions from the pre-active state 3 to the active state 4. Therefore, the stability of the pre-active state 3 is a critical tuner for setting the receptor activation threshold.

Discussion

GPCRs are evolved to transduce signals across the membrane through energetically passive allosteric mechanisms that involve communication between spatially separated and conformationally linked domains of the receptor[3]. For many multidomain GPCRs the mechanism of such conformational coupling and the dynamic interaction of the receptor domains during the allosteric process of activation are generally unknown. In this study, we successfully applied a new smFRET and live-cell ensemble FRET approach to visualize the temporal sequence of conformational changes of the CRD in mGluR2. The CRD is a unique semi-rigid structural domain, conserved among class C GPCRs (except $GABA_B$ receptors) that relay the conformational information of the VFT domains to the 7TM domains. The CRD of mGluRs has a compact structural fold with nine conserved cysteines. Therefore, conventional site-specific labeling approaches, such as cysteine labeling[13] or insertion of genetic tags[10], are not applicable. We adopted an unnatural amino acid-labeling approach[24] combined with single-molecule pulldown[29] to overcome this key limitation. Using this approach we found that the CRD in mGluR2 is in equilibrium between four conformations. An agonist 'loosely' controls the conformation of the ectodomains of the receptor, which in turn results in redistribution of the conformational ensemble and compaction of the receptor in a stepwise manner (Fig. 5). We observed the same four-state model for mGluR3, suggesting that this model could be general for all mGluRs (Extended Data Fig. 5). A recent cryo-electron microscopy study identified four conformations of the $GABA_B$ receptor[39], further suggesting that this four-state model could be the general activation model for all class C GPCRs. More broadly, other bi-lobed, clamshell ligand-binding domain-containing proteins, such as the ionotropic neurotransmitter receptors (NMDA, AMPA), may have evolved to utilize a similar activation mechanism.

Our model (Fig. 5) has several implications for the activation and modulation of mGluRs. First, we demonstrated that the activation proceeds through a conformational state where the VFT domain of only one subunit is active (state 2). Stalling the receptor in this state, which we achieved by mutations in the VFT domain of one subunit within the dimer, greatly hinders the progression of conformational changes of the receptor towards activation. Second, signaling of GPCRs in general, and of mGluRs specifically, can be modulated by endogenous or exogenous allosteric modulators (such as lipids or PAMs and NAMs)[3,40]. While synthetic allosteric modulators are attractive therapeutics, due to their superior specificity and tunability[40], their mechanism of action in class C GPCRs is unknown. Our analysis revealed that the PAM mutation C770A confers positive allosteric modulation by decreasing the lifetime of the new state 3 and by increasing transitions from state 3 to the active state 4, resulting in a greater overall occupancy of the active state (Fig. 4d,e and Extended Data Fig. 10b–d). Due to the stepwise compaction required for mGluR activation, several energetic barriers must be overcome to achieve receptor signaling. While each of these transitions may be modulable, we show that the C770A mutation specifically functions to reduce the barrier between states 3 and 4. Furthermore, the location of this mutation in TM6, the active 7TM domain interface[17,37], supports the possibility that a stabilizing 7TM domain interaction is necessary for the active receptor conformation (state 4). Together, the new intermediate states act as critical conformational checkpoints for regulating mGluR activation and signaling. These insights have the potential to accelerate development of drugs and modulators for mGluRs.

Third, we found that the active conformation of the receptor at the CRD is transient and dynamic, even in the presence of saturating full agonist (Figs. 2c and 3d and Extended Data Fig. 4b). This is in contrast to the behavior of the VFT domain of the receptor, which is very stable in saturating agonist[10] (Fig. 3d and Extended Data Fig. 3c). This could explain why, while there are several active structures of the extracellular domain of class C GPCRs available[17,18,27], obtaining the active structure of the 7TM domain in intact mGluRs has been challenging[17]. Finally, our results collectively suggest that mGluRs adopt a single active conformation, the stability of which is determined not only by ligand binding and closure of the VFT domains, but also by the propensity of the 7TM domains to interact within the dimer.

GPCR dimerization and oligomerization in vivo and in a ligand-dependent manner has been the subject of extensive research[41,42] and formation of GPCR dimers is shown to be transient and depends on agonist binding[43–45]. Our model raises the interesting possibility that class C GPCRs are evolved to use this intrinsic property to control their activation. In this framework, agonist binding effectively brings the 7TM domains into close proximity to facilitate their interaction and promote formation of the signaling-active configuration of the G protein-binding interface. This mechanism is, in essence, similar to many receptor tyrosine kinases[46], where ligand binding effectively controls the proximity of signaling or enzymatic domains, and may be the design principle underlying many biological allosteric switches.

Online content

Any methods, additional references, Nature Research reporting summaries, source data, extended data, supplementary information, acknowledgements, peer review information; details of author contributions and competing interests; and statements of data and code availability are available at https://doi.org/10.1038/s41589-020-00702-5.

Received: 3 February 2020; Accepted: 28 October 2020;
Published online: 4 January 2021

References

1. Smock, R. G. & Gierasch, L. M. Sending signals dynamically. *Science* **324**, 198–203 (2009).
2. Changeux, J. P. & Christopoulos, A. Allosteric modulation as a unifying mechanism for receptor function and regulation. *Cell* **166**, 1084–1102 (2016).
3. Thal, D. M., Glukhova, A., Sexton, P. M. & Christopoulos, A. Structural insights into G-protein-coupled receptor allostery. *Nature* **559**, 45–53 (2018).
4. Dorsam, R. T. & Gutkind, J. S. G-protein-coupled receptors and cancer. *Nat. Rev. Cancer* **7**, 79–94 (2007).
5. Zarzycka, B., Zaidi, S. A., Roth, B. L. & Katritch, V. Harnessing ion-binding sites for GPCR pharmacology. *Pharmacol. Rev.* **71**, 571–595 (2019).
6. Hilger, D., Masureel, M. & Kobilka, B. K. Structure and dynamics of GPCR signaling complexes. *Nat. Struct. Mol. Biol.* **25**, 4–12 (2018).
7. Latorraca, N. R., Venkatakrishnan, A. J. & Dror, R. O. GPCR dynamics: structures in motion. *Chem. Rev.* **117**, 139–155 (2017).
8. Ye, L., Van Eps, N., Zimmer, M., Ernst, O. P. & Prosser, R. S. Activation of the A2A adenosine G-protein-coupled receptor by conformational selection. *Nature* **533**, 265–268 (2016).
9. Nygaard, R. et al. The dynamic process of β_2-adrenergic receptor activation. *Cell* **152**, 532–542 (2013).
10. Vafabakhsh, R., Levitz, J. & Isacoff, E. Y. Conformational dynamics of a class C G-protein-coupled receptor. *Nature* **524**, 497–501 (2015).
11. Wingler, L. M. et al. Angiotensin analogs with divergent bias stabilize distinct receptor conformations. *Cell* **176**, 468–478 (2019).
12. Gusach, A. et al. Beyond structure: emerging approaches to study GPCR dynamics. *Curr. Opin. Struct. Biol.* **63**, 18–25 (2020).
13. Gregorio, G. G. et al. Single-molecule analysis of ligand efficacy in β_2AR–G-protein activation. *Nature* **547**, 68–73 (2017).
14. Suomivuori, C. M. et al. Molecular mechanism of biased signaling in a prototypical G protein-coupled receptor. *Science* **367**, 881–887 (2020).
15. Niswender, C. M. & Conn, P. J. Metabotropic glutamate receptors: physiology, pharmacology, and disease. *Annu. Rev. Pharmacol. Toxicol.* **50**, 295–322 (2010).
16. Pin, J. P. & Bettler, B. Organization and functions of mGlu and $GABA_B$ receptor complexes. *Nature* **540**, 60–68 (2016).
17. Koehl, A. et al. Structural insights into the activation of metabotropic glutamate receptors. *Nature* **567**, 79–84 (2019).
18. Kunishima, N. et al. Structural basis of glutamate recognition by a dimeric metabotropic glutamate receptor. *Nature* **407**, 971–977 (2000).
19. Wu, H. et al. Structure of a class C GPCR metabotropic glutamate receptor 1 bound to an allosteric modulator. *Science* **344**, 58–64 (2014).
20. Doumazane, E. et al. Illuminating the activation mechanisms and allosteric properties of metabotropic glutamate receptors. *Proc. Natl Acad. Sci. USA* **110**, E1416–E1425 (2013).
21. Hlavackova, V. et al. Sequential inter- and intrasubunit rearrangements during activation of dimeric metabotropic glutamate receptor 1. *Sci. Signal.* **5**, ra59 (2012).
22. Roy, R., Hohng, S. & Ha, T. A practical guide to single-molecule FRET. *Nat. Methods* **5**, 507–516 (2008).
23. Noren, C. J., Anthony-Cahill, S. J., Griffith, M. C. & Schultz, P. G. A general-method for site-specific incorporation of unnatural amino-acids into proteins. *Science* **244**, 182–188 (1989).
24. Serfling, R. & Coin, I. Incorporation of unnatural amino acids into proteins expressed in mammalian cells. *Methods Enzymol.* **580**, 89–107 (2016).
25. Huber, T., Naganathan, S., Tian, H., Ye, S. X. & Sakmar, T. P. Unnatural amino acid mutagenesis of GPCRs using amber codon suppression and bioorthogonal labeling. *Method Enzymol.* **520**, 281–305 (2013).
26. Presolski, S. I., Hong, V. P. & Finn, M. G. Copper-catalyzed azide-alkyne click chemistry for bioconjugation. *Curr. Protoc. Chem. Biol.* **3**, 153–162 (2011).
27. Muto, T., Tsuchiya, D., Morikawa, K. & Jingami, H. Structures of the extracellular regions of the group II/III metabotropic glutamate receptors. *Proc. Natl. Acad Sci. USA* **104**, 3759–3764 (2007).
28. Huang, S. L. et al. Interdomain movements in metabotropic glutamate receptor activation. *Proc. Natl Acad. Sci. USA* **108**, 15480–15485 (2011).
29. Jain, A. et al. Probing cellular protein complexes using single-molecule pull-down. *Nature* **473**, 484–488 (2011).
30. Bronson, J. E., Fei, J., Hofman, J. M., Gonzalez, R. L. Jr. & Wiggins, C. H. Learning rates and states from biophysical time series: a Bayesian approach to model selection and single-molecule FRET data. *Biophys. J.* **97**, 3196–3205 (2009).
31. Zhang, J. et al. Specific structural elements of the T-box riboswitch drive the two-step binding of the tRNA ligand. *Elife* **7**, e39518 (2018).
32. Nussinov, R., Ma, B. & Tsai, C. J. Multiple conformational selection and induced fit events take place in allosteric propagation. *Biophys. Chem.* **186**, 22–30 (2014).
33. Manglik, A. et al. Structural insights into the dynamic process of β_2-adrenergic receptor signaling. *Cell* **161**, 1101–1111 (2015).
34. Dror, R. O. et al. Activation mechanism of the β_2-adrenergic receptor. *Proc. Natl. Acad. Sci. USA* **108**, 18684–18689 (2011).
35. Grushevskyi, E. O. et al. Stepwise activation of a class C GPCR begins with millisecond dimer rearrangement. *Proc. Natl Acad. Sci. USA* **116**, 10150–10155 (2019).
36. Kniazeff, J. et al. Closed state of both binding domains of homodimeric mGlu receptors is required for full activity. *Nat. Struct. Mol. Biol.* **11**, 706–713 (2004).
37. Xue, L. et al. Major ligand-induced rearrangement of the heptahelical domain interface in a GPCR dimer. *Nat. Chem. Biol.* **11**, 134–140 (2015).
38. Yanagawa, M., Yamashita, T. & Shichida, Y. Activation switch in the transmembrane domain of metabotropic glutamate receptor. *Mol. Pharmacol.* **76**, 201–207 (2009).
39. Shaye, H. et al. Structural basis of the activation of a metabotropic GABA receptor. *Nature* **584**, 298–303 (2020).
40. Foster, D. J. & Conn, P. J. Allosteric modulation of GPCRs: new insights and potential utility for treatment of schizophrenia and other CNS disorders. *Neuron* **94**, 431–446 (2017).
41. Mijares, A., Lebesgue, D., Wallukat, G. & Hoebeke, J. From agonist to antagonist: Fab fragments of an agonist-like monoclonal anti-β_2-adrenoceptor antibody behave as antagonists. *Mol. Pharmacol.* **58**, 373–379 (2000).
42. Stoneman, M. R. et al. A general method to quantify ligand-driven oligomerization from fluorescence-based images. *Nat. Methods* **16**, 493–496 (2019).
43. Hern, J. A. et al. Formation and dissociation of M1 muscarinic receptor dimers seen by total internal reflection fluorescence imaging of single molecules. *Proc. Natl Acad. Sci. USA* **107**, 2693–2698 (2010).
44. Calebiro, D. et al. Single-molecule analysis of fluorescently labeled G-protein-coupled receptors reveals complexes with distinct dynamics and organization. *Proc. Natl Acad. Sci. USA* **110**, 743–748 (2013).
45. Moller, J. et al. Single-molecule analysis reveals agonist-specific dimer formation of μ-opioid receptors. *Nat. Chem. Biol.* **16**, 946–954 (2020).
46. Endres, N. F. et al. Conformational coupling across the plasma membrane in activation of the EGF receptor. *Cell* **152**, 543–556 (2013).

Methods

Molecular cloning. The C-terminal FLAG-tagged mouse mGluR2 and mGluR3 constructs in pcDNA3.1$^+$ expression vector were purchased from GenScript (ORF clone: OMu19627D and OMu17682D) and verified by sequencing (ACGT). The mutation of amino acid A548 in mGluR2 and A557 in mGluR3 to an amber codon (TAG) was performed using the QuikChange site-directed mutagenesis kit (Qiagen). The same approach was used to introduce point mutations in mGluR2 (Y216A, D295A, C770A and L521C) for other experiments. For the YADA/WT mGluR2 (548UAA) heterodimer experiment, a SNAP-tag ($pSNAP_f$, NEB) was inserted at position 19, flanked by GGS linkers, using HiFi DNA Assembly Master Mix (NEB). Finally, site-directed mutagenesis was done to remove the C-terminal FLAG-tag on this construct. All plasmids were sequence verified (ACGT). DNA restriction enzymes, DNA polymerase and DNA ligase were from New England Biolabs. Plasmid preparation kits were purchased from Macherey-Nagel.

Cell culture conditions. HEK293T cells were purchased from Sigma and were maintained in DMEM (Corning) supplemented with 10% (v/v) fetal bovine serum (GE Healthcare), 100 unit ml^{-1} penicillin–streptomycin (Gibco) and 15 mM HEPES (pH 7.4, Gibco) at 37 °C under 5% CO_2. The cells were passaged with 0.05% trypsin–EDTA (Gibco). For unnatural amino acid-containing protein expression, the growth media were supplemented with 0.6 mM 4-azido-L-phenylalanine (Chem-Impex International). All media were filtered by 0.2 µM PES filters (Fisher Scientific).

Transfection and protein expression. At 24 h before transfection, HEK293T cells were cultured in 10-cm cell culture dishes (Corning) or polylysine-coated 18-mm glass coverslips (VWR). One hour before transfection, medium was changed to growth medium, supplemented with 0.6 mM 4-azido-L-phenylalanine. mGluR plasmids as described above and pIRE4-Azi plasmid (pIRE4-Azi was a gift from I. Coin, Addgene plasmid no. 105829) were cotransfected (1:1 w/w) into cells using Transporter 5 (Polysciences) or Lipofectamine 3000 (Invitrogen) (total plasmid: 1.5 µg per 18-mm coverslip). For YADA/WT heterodimer experiments, SNAP-548UAA(WT), pIRE4-Azi and 548UAA YADA were cotransfected (1:1:1 w/w/w) using Transporter 5 (Polysciences) (total plasmid: 2 µg per 18-mm coverslip). The growth medium containing 0.6 mM 4-azido-L-phenylalanine was refreshed after 24 h and the cells were grown for another 24 h (total 48 h expression). On the day of the experiment, 10 min before labeling, supplemented growth medium was removed and cells were washed twice by extracellular buffer solution containing (in mM): 128 NaCl, 2 KCl, 2.5 $CaCl_2$, 1.2 $MgCl_2$, 10 sucrose, 10 HEPES, pH 7.4 and were kept in growth medium without 4-azido-L-phenylalanine. Before the addition of labeling solution (below), cells were washed once with extracellular buffer solution.

SNAP-tag labeling in live cells. SNAP labeling of the N terminus VFT domain (Extended Data Fig. 3c) was done by incubating the cells with 4 µM of benzylguanine Alexa-647 (NEB) and 4 µM of benzylguanine DY-549P1 (NEB) in extracellular buffer for 30 min at 37 °C. SNAP labeling for the YADA/WT heterodimer experiments (Fig. 3e,f and Extended Data Fig. 9) was done at 37 °C with 4 µM of SNAP-Surface ATTO488 (NEB) in extracellular buffer for 30 min. After labeling, the coverslip was gently washed twice in extracellular buffer to remove excess dye.

Unnatural amino acid labeling in live cells by azide-alkyne click chemistry. A modified version of previously reported protocols[26,47] was used to fluorescently label the incorporated 4-azido-L-phenylalanine in live cells. Stock solutions were made as follows: Cy3 and Cy5 alkyne dyes (Click Chemistry Tools) 10 mM in DMSO, BTTES (Click Chemistry Tools) 50 mM, copper sulfate (Millipore Sigma) 20 mM, aminoguanidine (Cayman Chemical) 100 mM and (+)-sodium L-ascorbate (Millipore Sigma) 100 mM in ultrapure distilled water (Invitrogen). In 656 µl of extracellular buffer solution, Cy3 and Cy5 alkyne dyes were mixed to a final concentration of 18 µM of each dye. To this mixture, a fresh premixed solution of copper sulfate and BTTES (1:5 molar ratio) was added at the final concentration of 150 µM and 750 µM, respectively. Next, aminoguanidine was added to a final concentration of 1.25 mM and (+)-sodium L-ascorbate was added to the mixture to a final concentration of 2.5 mM. The total labeling volume was 0.7 ml. The labeling mixture was kept at 4 °C for 8 min followed by 2 min at room temperature before addition to the cells. Cells were washed before addition of the labeling mixture. During labeling, cells were kept in the dark at 37 °C and 5% CO_2. After 10 min, L-glutamate (Sigma) was added to the cells to a final concentration of 0.5 mM and cells were incubated for an additional 5 min. After labeling, cells were washed twice with extracellular buffer. For the gel electrophoresis experiment, only Cy5 alkyne dye was used with the final concentration of 35 µM.

Gel electrophoresis. After labeling, cells from three 10-cm dishes were washed with extracellular buffer and detached from the plates by incubating with Ca^{2+}-free DPBS (Thermo Scientific) buffer, followed by a gentle pipetting. Cells were then pelleted by centrifugation at 4,000*g* and 4 °C for 10 min. The pellet was lysed in 1.5 ml lysis buffer (pH 7.2) consisting of 200 mM NaCl, 50 mM HEPES, 1 mM EDTA, protease inhibitor tablet (ThermoFisher Scientific) and 1% DDM-CHS (10:1, Anatrace). After 1 h of gentle mixing at 4 °C, cells were centrifuged at 20,000*g* and 4 °C for 20 min and the supernatant was collected and concentrated to 150 µl using 100-kDa centrifugal filters (Millipore) at 4 °C. A 10-µl portion of this solution was mixed with 10 µl of 50% glycerol and loaded into a precast 4–20 % gradient nonreducing polyacrylamide gel (Bio-Rad) and run at 100 V for 45 min. A 2-µl portion of precision plus protein standard (Bio-Rad) was used as a ladder. The gel was washed two times in ultrapure water and the image was captured using a Typhoon 9400 fluorimager (GE Healthcare) with 633-nm excitation wavelength and a 670-BP30 emission filter.

Confocal microscopy. Live-cell images were acquired using an inverted confocal microscope (Zeiss, LSM-800) with a ×40 oil-immersion objective, equipped with 561 and 640 nm lasers, with two GaAsP-PMT detectors with detection wavelengths of 540–617 nm and 645–700 nm for Cy3 and Cy5 channels, respectively.

Live-cell FRET measurements. After labeling, the coverslip was assembled in a flow chamber (Innova Plex) and attached to a gravity flow control system (ALA Scientific Instruments) to control buffer application during experiments. Buffers were applied at the rate of 5 ml min^{-1}. Labeled cells were imaged on a home-built total internal reflection fluorescence (TIRF) microscope equipped with a ×20 objective (Olympus, oil-immersion) in the oblique illumination mode and using an excitation filter set with a quad-edge dichroic mirror (Di03-R405/488/532/635, Semrock) and a long-pass filter (ET542lp, Chroma).

Cy3 (donor) was excited with a 532-nm laser (RPMC Lasers) and emissions from Cy3 and Cy5 fluorophores were simultaneously recorded with an electron multiplying charge-coupled device (EMCCD, iXon Ultra, Andor). All data were recorded at 4,500 ms time resolution. In the emission path a quad-notch filter (NF01-405/488/532/635, Semrock) was used to block lasers and a dichroic beamsplitter (FF640-FDi01, Semrock) was used to split the emission into donor and acceptor signals.

Movies were analyzed in Fiji[48] by manually drawing a region of interest (ROI) around the membrane of each analyzed cell. Built-in Fiji functions were used to calculate the mean gray intensity within the ROIs in both donor and acceptor channels and over all the frames. Donor and acceptor intensities were corrected for background, which was measured from a region in the same field of view and without cells. The acceptor intensity was corrected for bleed through of the Cy3 donor signal into the Cy5 acceptor channel, which we measured to be 8.8% of the Cy3 intensity in our setup. Apparent FRET efficiency was calculated as $FRET = (I_A - 0.088I_D)/(I_D + I_A)$, where I_D and I_A are the background-corrected donor and acceptor intensities, respectively. Cells and ROIs were inspected for lack of substantial drift, lateral movement and the presence of anticorrelated behavior of donor and acceptor signals.

During the titration experiments the wash buffer or buffers containing the specified ligand were continuously applied long enough for the FRET curve to stabilize and plateau. To calculate the FRET change (ΔFRET) for each ligand application, the average of FRET efficiency for six data points before the application of ligand was calculated and assigned as FRET_before. The average FRET efficiency for six data points after the application of ligand and after the FRET curve has plateaued was calculated and assigned as FRET_after. FRET change (ΔFRET) was calculated as ΔFRET = FRET_after − FRET_before. Dose–response equation $y(x) = A1 + \frac{A2-A1}{1+10^{((\log x_0 - x)P}}$ was used for fitting ΔFRET data to calculate EC_{50} values, where *A1* is the lower asymptote, *A2* is the upper asymptote, *P* is the Hill slope and x_0 is the EC_{50}.

DCG-IV and Ro64-5229 were purchased from Tocris. LY379268 was purchased from Cayman Chemical. All curve fittings were done in OriginPro (OriginLab).

Structural analysis. Distances were measured in Chimera[49]. On the basis of the spectral overlap of Cy3 alkyne and Cy5 alkyne, a Förster radius (R_0) of 55 Å was used to convert raw FRET efficiency (*F*) to an approximate distance using $FRET = 1/(1 + (R/R_0)^6)$. Figure 1a was created using Illustrate[50].

Single-molecule FRET measurements. Single-molecule FRET experiments were done in flow cells that were prepared using glass coverslips (VWR) and slides (ThermoFisher Scientific) passivated with mPEG (Laysan Bio) and 1% (w/w) biotin-PEG to prevent unspecific protein adsorption, as previously described[10,51]. Before experiments, flow cells were first incubated with 500 nM NeutrAvidin (ThermoFisher Scientific) for 2 min followed by 20 µM biotinylated FLAG antibody (A01429, GenScript) for 30 min. Unbound NeutrAvidin and biotinylated FLAG antibody were removed by washing. Washes and protein dilutions were done with T50 buffer (50 mM NaCl, 10 mM Tris, pH 7.4).

After labeling, cells were recovered from a single 10-cm plate by incubating with Ca^{2+}-free DPBS followed by gentle pipetting. Cells were then pelleted by centrifugation at 4,000*g* and 4 °C for 10 min. The cell pellet was lysed in 350 µl of lysis buffer consisting of 200 mM NaCl, 50 mM HEPES, 1 mM EDTA, protease inhibitor tablet (ThermoFisher Scientific) and 1% DDM-CHS (10:1, Anatrace), pH 7.2. After 1 h of gentle mixing at 4 °C, lysate was centrifuged at 20,000*g* and 4 °C for 20 min. The supernatant was collected and diluted (five- to tenfold dilution depending on the concentration) and was then added to the flow chamber to achieve sparse surface immobilization of labeled receptors

by their C-terminal FLAG-tag. Sample dilution and washes were done using a dilution buffer consisting of 200 mM NaCl, 50 mM HEPES and 0.1% DDM-CHS (10:1, Anatrace), pH 7.2. After optimal receptor coverage was achieved, the flow chamber was washed extensively with dilution buffer to remove unbound proteins (>20× chamber volume). Finally, labeled receptors were imaged in imaging buffer consisting of (in mM): 4 Trolox, 128 NaCl, 2 KCl, 2.5 $CaCl_2$, 1.2 $MgCl_2$, 40 HEPES, 0.05% DDM-CHS (10:1) and an oxygen-scavenging system consisting of 4 mM protocatechuic acid (Sigma) and 1.6 U ml^{-1} bacterial protocatechuate 3,4-dioxygenase (rPCO) (Oriental Yeast), pH 7.35. All reagents were prepared from ultrapure-grade chemicals (purity >99.99%) and were purchased from Sigma. All buffers were made using ultrapure distilled water (Invitrogen).

Samples were imaged with a ×100 objective (Olympus, 1.49 numerical aperture, oil-immersion) on a TIRF microscope, as described above, with 30 ms time resolution unless stated otherwise (Extended Data Fig. 3a). Lasers at 532 nm and 638 nm (RPMC Lasers) were used for donor and acceptor excitation, respectively. For the YADA/WT mGluR2 heterodimer experiments, a 488-nm laser was used to excite receptors labeled by SNAP (BG-ATTO488), before excitation with lasers at 532 nm and 638 nm (Extended Data Fig. 9).

smFRET data analysis. Analysis of single-molecule fluorescence data was performed using smCamera (http://ha.med.jhmi.edu/resources/), custom MATLAB (MathWorks) scripts and OriginPro (OriginLab). Particle selection and generation of raw FRET traces were done automatically within the smCamera software (Extended Data Fig. 3a). For the selection, particles that showed acceptor signal upon donor excitation, with acceptor brightness greater than 10% above background and that had a Gaussian intensity profile, were automatically selected, and donor and acceptor intensities were measured over all the frames. From this pool, particles that showed a single donor and a single acceptor bleaching step during the acquisition time, stable total intensity ($I_D + I_A$), anticorrelated donor and acceptor intensity behavior without blinking events and that lasted for more than 4 s were manually selected for further analysis (~20%–30% of total molecules per movie). All data were analyzed by three individuals independently and the results were compared and shown to be identical. In addition, a subset of data was analyzed blind to ensure no bias in the analysis. Apparent FRET efficiency was calculated as $(I_A - 0.088I_D)/(I_D + I_A)$, where I_D and I_A are raw donor and acceptor intensities, respectively. For the YADA/WT mGluR2 heterodimer experiments, identity of heterodimers was confirmed by observing a single photobleaching event upon 488-nm laser excitation. All experiments were repeated at least three times independently to ensure reproducibility of the results. Population smFRET histograms were generated by compiling at least 200 FRET traces from individual molecules unless otherwise stated. Before compiling traces, FRET histograms of individual molecules were normalized to 1 to ensure that each trace contributed equally, regardless of trace length. Error bars on histograms represent the standard error of at least six independent movies.

Peak fitting on population smFRET histograms was performed using OriginPro and using four Gaussian distributions as $\boldsymbol{y}(\boldsymbol{x}) = \sum_{i=1}^{4} \frac{A_i}{w_i\sqrt{\frac{\pi}{2}}} e^{-2\frac{(x-xc_i)^2}{w_i^2}}$, where A is the peak area, xc is the FRET peak center and w is the peak width for each peak. Peak centers (xc) were constrained as mean FRET efficiency of a conformational state ±0.02. The mean FRET efficiencies of the four conformations were determined on the basis of the most frequent FRET states observed in transition density plots. This analysis is further described below. Peak widths were constrained as $0.1 \leq w \leq 0.24$. Peak areas were constrained as $A > 0$. Probability of state occupancy was calculated as area of specified peaks relative to the total area, which is defined as the sum of all four individual peak areas.

Raw donor, acceptor and FRET traces were idealized by fitting with a hidden Markov model (HMM) using vbFRET software[30,31]. Transition density plots were then generated by extracting all the transitions where ΔFRET > 0.1 from the idealized traces. Occasional traces for which the HMM fit did not converge (for example, due to long blinking events or large non-anticorrelated intensity fluctuations) were omitted from downstream analysis.

The idealized FRET traces were also used to calculate the dwell times for each of the four states. A total of 147, 140, 128 and 142 molecules from three independent measurements were used for dwell-time analysis of states 3 and 4 for UAA548 (5 µM and 10 µM glutamate) and mGluR2 C770A (5 µM and 10 µM glutamate), respectively. A total of 86, 83, 91 and 72 molecules from two independent measurements were used for dwell-time analysis of states 1 and 2 for the same respective constructs and conditions. Reported values represent mean, and error bars represent s.e.m. At least 350 transitions were analyzed for each condition. The dwell times were plotted as cumulative-count histograms and were fit with a single exponential decay function $y(x) = y_0 + A_1 e^{-x/\tau}$ by OriginPro (OriginLab).

The cross-correlation (CC) of donor and acceptor intensity traces at time τ is defined as $CC(\tau) = \delta I_D(t)\delta I_A(t+\tau)/(<I_D(t)> + <I_A(t)>)$, where $\delta I_D(t) = I_D(t) - <I_D(t)>$, and $\delta I_A(t) = I_A(t) - <I_A(t)>$. $<I_D(t)>$ and $<I_D(t)>$ are time average donor and acceptor intensities, respectively. Cross-correlation calculations were performed on the same traces used to generate the histograms. Cross-correlation data were fit to a single exponential function.

Reporting Summary. Further information on research design is available in the Nature Research Reporting Summary linked to this article.

Data availability

The materials and data reported in this study are available from the corresponding author upon reasonable request. The PDB accession codes for the inactive and active structures of human mGluR5 are 6N52 and 6N51. Source data are provided with this paper.

Code availability

The custom codes for data analysis are available from the corresponding author upon reasonable request.

References

47. Hong, V., Steinmetz, N. F., Manchester, M. & Finn, M. G. Labeling live cells by copper-catalyzed alkyne–azide click chemistry. *Bioconjug. Chem.* **21**, 1912–1916 (2010).
48. Schindelin, J. et al. Fiji: an open-source platform for biological-image analysis. *Nat. Methods* **9**, 676–682 (2012).
49. Pettersen, E. F. et al. UCSF Chimera—a visualization system for exploratory research and analysis. *J. Comput. Chem.* **25**, 1605–1612 (2004).
50. Goodsell, D. S., Autin, L. & Olson, A. J. Illustrate: software for biomolecular illustration. *Structure* **27**, 1716–1720 (2019).
51. Jain, A., Liu, R., Xiang, Y. K. & Ha, T. Single-molecule pull-down for studying protein interactions. *Nat. Protoc.* **7**, 445–452 (2012).

Acknowledgements

We thank M.R. Schamber, D. Badong, D. May and A.Y. Pen for technical assistance, M. Gallio, J. Marko, A. Mondragon and K. Ragunathan for critical reading of the manuscript, and J. Fei (University of Chicago) for providing MATLAB scripts. This work was supported by the National Institutes of Health grant R01GM140272 (to R.V.) and by The Searle Leadership Fund for the Life Sciences at Northwestern University and by the Chicago Biomedical Consortium with support from the Searle Funds at The Chicago Community Trust (to R.V.). B.W.L. was supported by the National Institute of General Medical Sciences (NIGMS) Training Grant T32GM-008061. This work used resources of the Keck Biophysics Facility supported in part by the NCI CCSG P30 CA060553 grant awarded to the Robert H. Lurie Comprehensive Cancer Center of Northwestern University.

Author contributions

B.W.L. performed plasmid construction and smFRET experiments. H.S.A. optimized and performed unnatural amino acid labeling and verification and live-cell FRET imaging and analysis. B.W.L. performed smFRET data analysis with assistance from H.S.A and R.V. The paper was written by B.W.L., H.S.A. and R.V.

Competing interests

The authors declare no competing interests.

Additional information

Extended data is available for this paper at https://doi.org/10.1038/s41589-020-00702-5.

Supplementary information is available for this paper at https://doi.org/10.1038/s41589-020-00702-5.

Correspondence and requests for materials should be addressed to R.V.

Reprints and permissions information is available at www.nature.com/reprints.

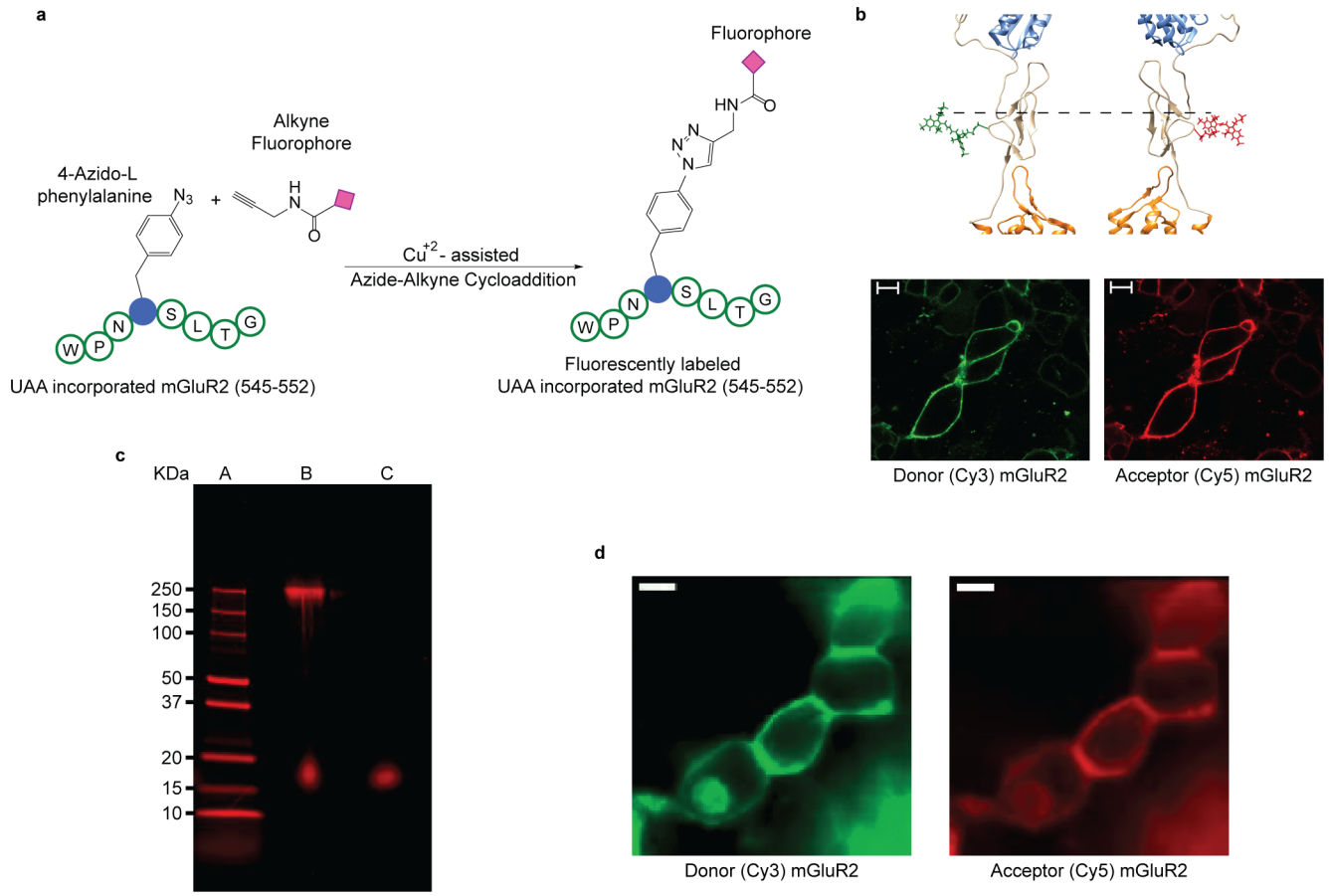

Extended Data Fig. 1 | Site-specific labeling of mGluR2 by click chemistry. a, Schematic showing site-specific fluorescent labeling of mGluR2, with the unnatural amino acid 4-azido-L-phenylalanine at residue 548, by copper-catalyzed azide-alkyne click reaction. **b**, Donor (green: Cy3) and acceptor (red: Cy5) fluorophores conjugated to the CRD of inactive mGluR5 (PDB 6N52) at the position corresponding to residue 548 in mGluR2 (top). Representative confocal microscope image of HEK293T cells expressing 548UAA with the cell surface population labeled with donor (green: Cy3) and acceptor (red: Cy5) fluorophores through click chemistry (bottom). Scale bars, 10 μm. **c**, Unprocessed image of non-reducing 4-20% polyacrylamide gel electrophoresis of cell lysate from HEK293T cells expressing 548UAA and labeled by Cy5-alkyne. The gel is imaged with 633 nm excitation wavelength and 670-BP30 emission filter. Lane A: protein ladder; lane B: cell lysate; lane C: Cy5-alkyne dye. Results are representative of an individual experiment. **d**, Image of HEK293T cells expressing 548UAA and labeled with donor (green: Cy3) and acceptor (red: Cy5) fluorophores through click chemistry during live-cell FRET experiments. Scale bars, 10 μm. Results are representative of all titration and max response experiments for the 548UAA construct (N=21 independent experiments).

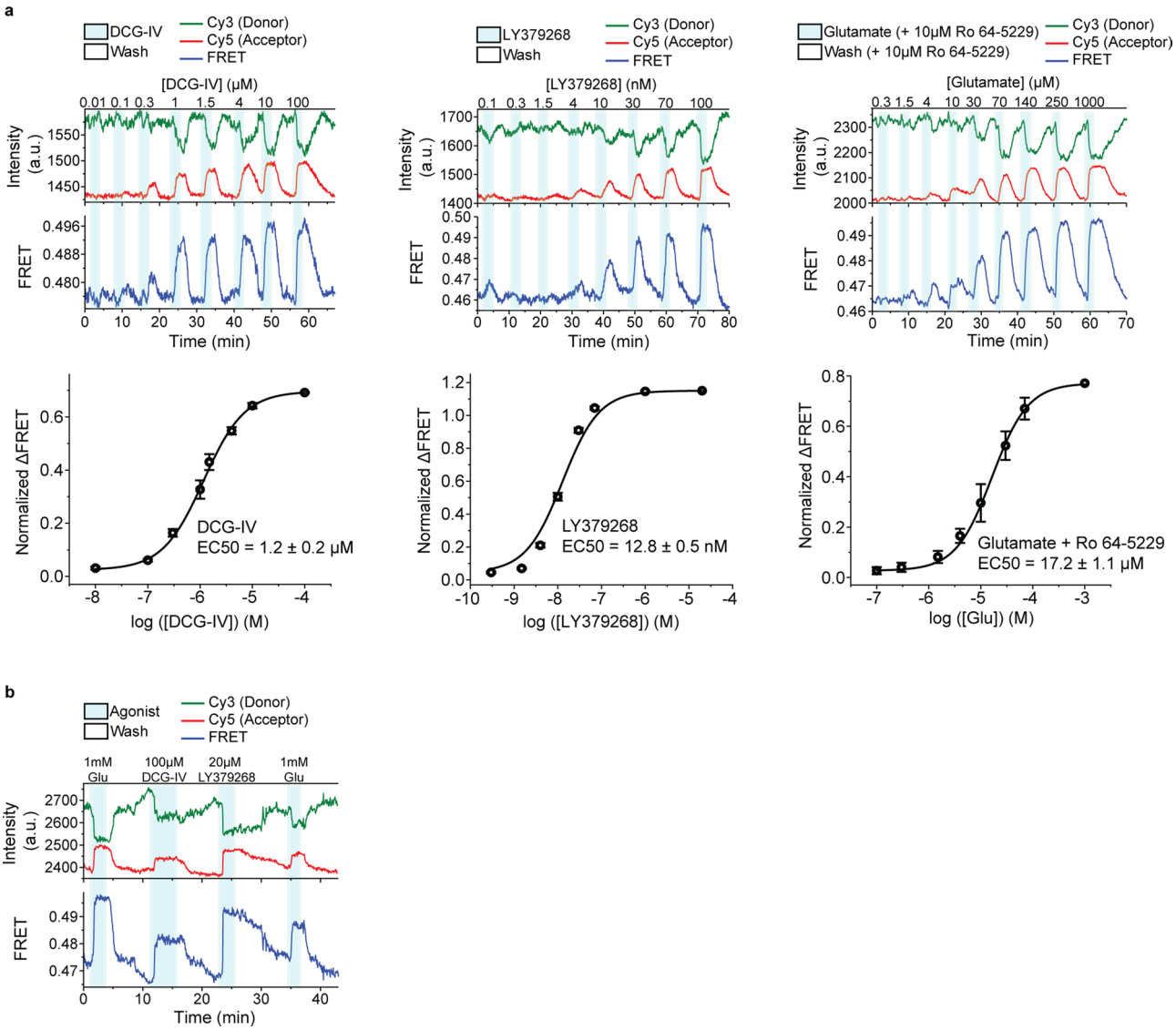

Extended Data Fig. 2 | Live-cell ensemble FRET response to orthosteric ligands and a negative allosteric modulator. a, Representative donor and acceptor intensities and corresponding FRET signal from live-cell FRET titration experiments for DCG-IV, LY379268 and Glutamate +10 μM Ro64-5229 measured using HEK293T cells expressing 548UAA (top) and corresponding dose-response curves (bottom). Each titration curve is normalized to the 1 mM glutamate response. Data represent mean ± s.e.m. of N=20, 10 and 13 cells for LY379268, DCG-IV and glutamate +10 μM Ro64-5229, respectively, examined over 3 independent experiments. **b**, Donor and acceptor intensities and corresponding FRET signal in response to saturating concentrations of glutamate (1 mM), DCG-IV (100 μM) and LY379268 (20 μM) in HEK293T cells expressing 548UAA.

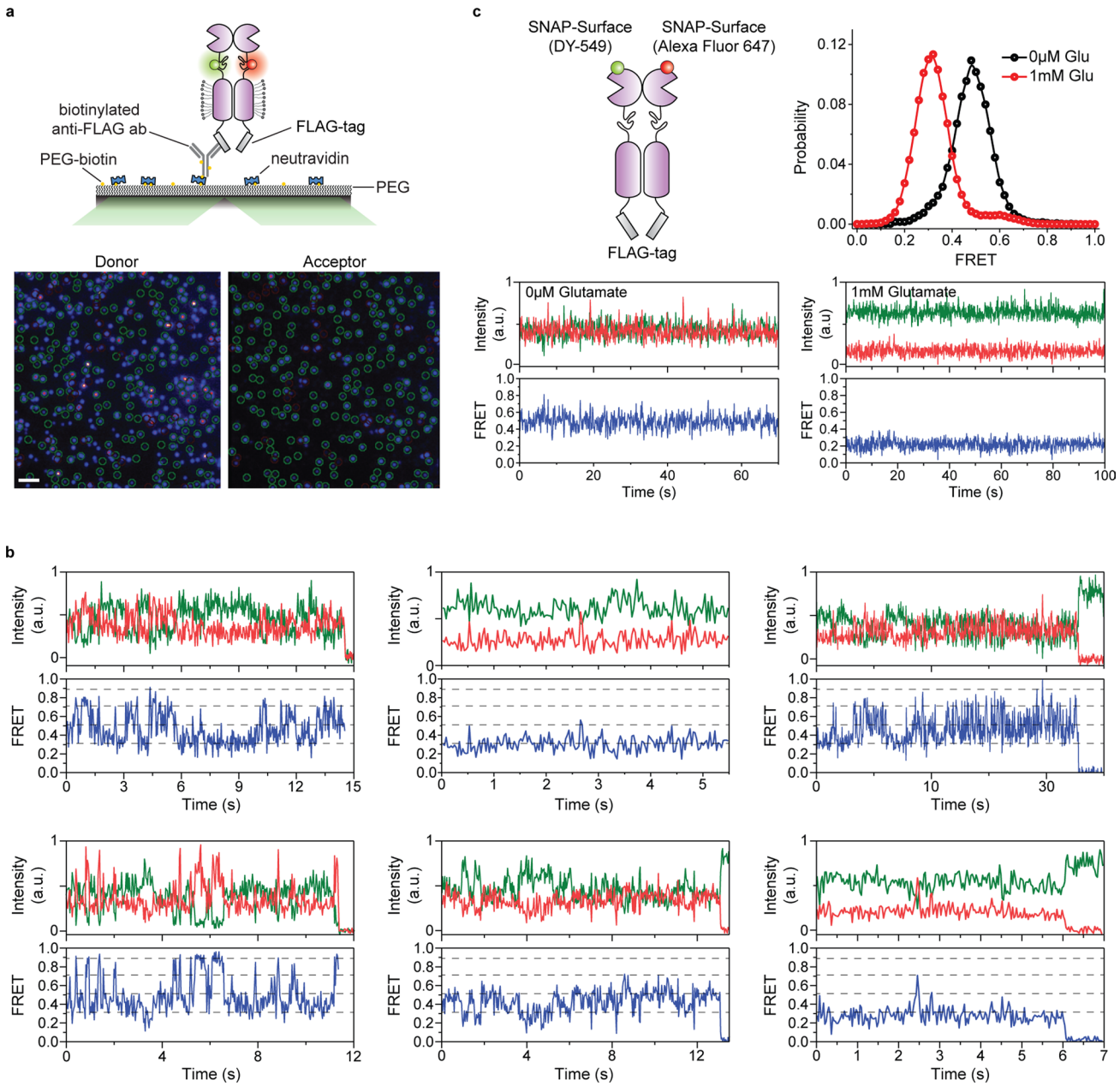

Extended Data Fig. 3 | Example single-molecule time traces of CRD and VFT domain sensors. a, Schematic of the single-molecule experiments (top). Representative frame from a single-molecule movie with the donor channel (Cy3) on the left and acceptor channel (Cy5) on the right (bottom). Molecules selected by analysis software for downstream processing are indicated by green circles. Scale bar, 3 μm. **b**, Example single-molecule time traces of the 548UAA in the absence of glutamate (0 μM) showing donor (green) and acceptor (red) intensities and corresponding FRET (blue). Dashed lines represent 4 distinct FRET states. **c**, Schematic of the VFT domain conformational sensor (left). Example single-molecule time traces of VFT domain sensor in the absence of glutamate (0 μM) and presence of saturating glutamate (1 mM) showing donor (green) and acceptor (red) intensities and corresponding FRET (blue) (bottom). smFRET population histogram of VFT domain mGluR2 sensor in the inactive (0 μM glutamate; 36 total molecules) and fully active (1 mM glutamate; 24 total molecules) conditions (top right). Data represent mean of N=2 independent experiments.

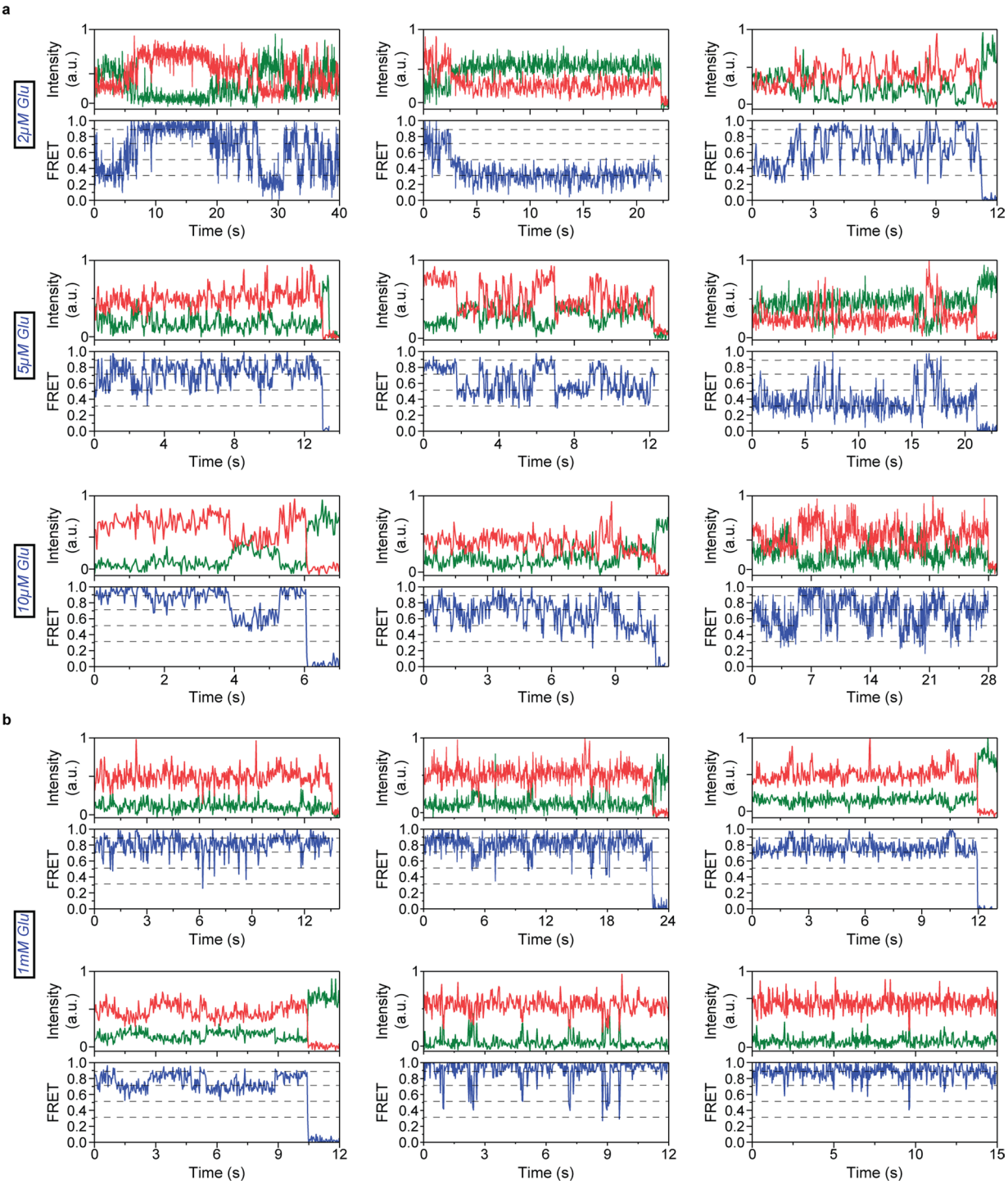

Extended Data Fig. 4 | Example single-molecule time traces of CRD at different glutamate concentrations. a, Example single-molecule time traces of the 548UAA at intermediate glutamate concentrations. **b**, Example single-molecule time traces of the 548UAA in saturating glutamate (1 mM). Donor (green) and acceptor (red) intensities and corresponding FRET (blue) are shown. Dashed lines represent 4 distinct FRET states.

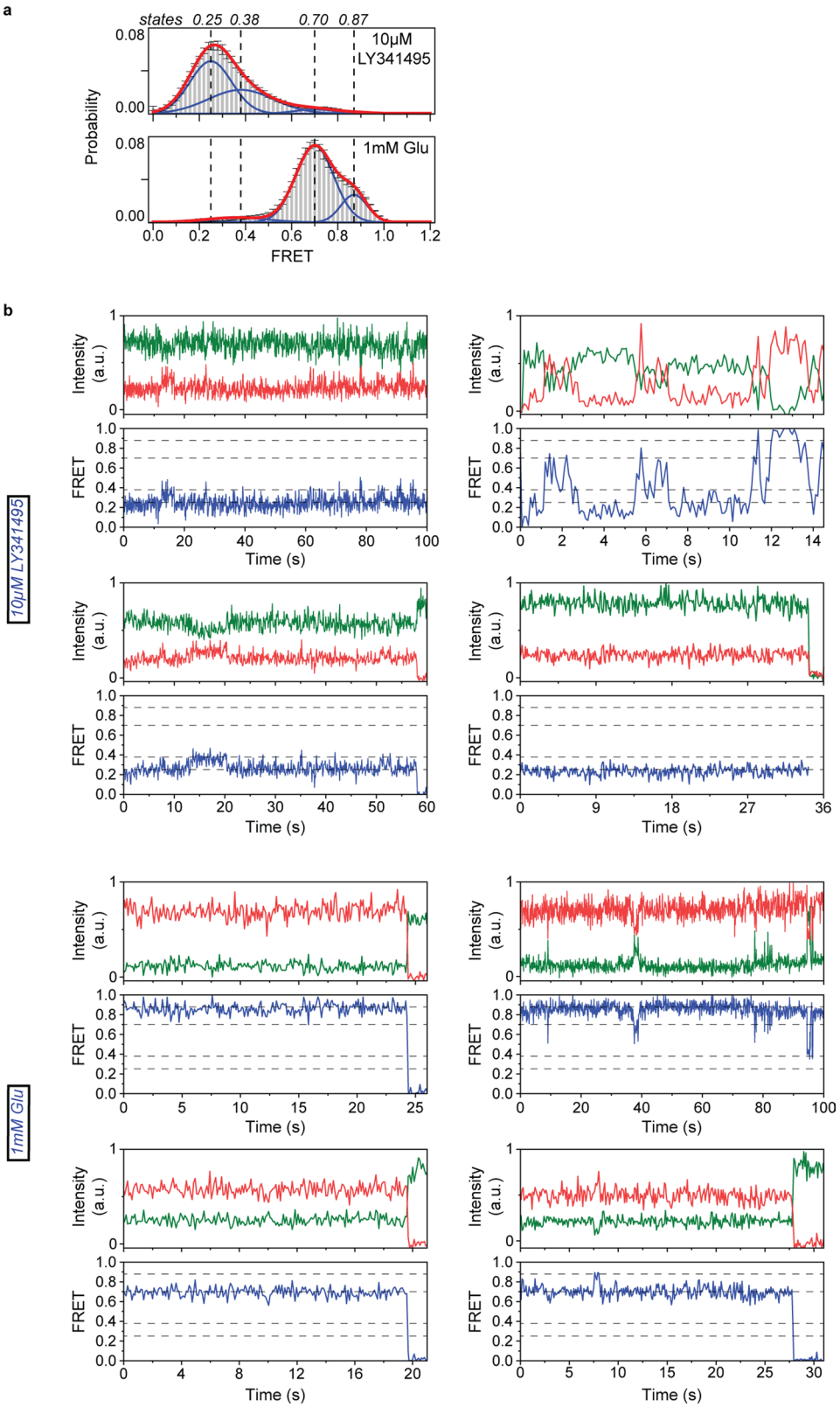

Extended Data Fig. 5 | mGluR3 undergoes a 4-state activation process. a, smFRET population histograms of mGluR3 CRD sensor (labeled at residue 557) in the presence of competitive antagonist (LY341495; 221 total molecules) or saturating glutamate (290 total molecules). Data represent mean ± s.e.m. of N=3 independent experiments. Histograms are fitted (red) to 4 Gaussian distributions (blue) centered around 0.25 (state 1), 0.38 (state 2), 0.7 (state 3) and 0.87 (state 4), denoted with dashed lines. **b**, Example single-molecule time traces of mGluR3 CRD sensor in the presence of antagonist (LY341495) or saturating glutamate (1 mM) showing donor (green) and acceptor (red) intensities and corresponding FRET (blue). Dashed lines represent 4 distinct FRET states. Data was acquired at 100 ms time resolution.

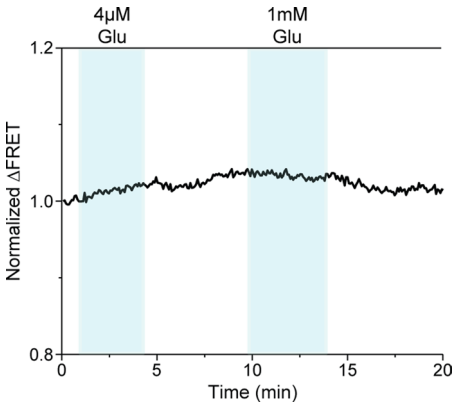

Extended Data Fig. 6 | Effect of intersubunit crosslinking on the CRD conformation. Representative live-cell FRET measurement using HEK293T cells expressing 548UAA with the crosslinking mutation L521C upon application of intermediate (4 μM) and saturating glutamate (1 mM). FRET signal is normalized using initial FRET at time = 0.

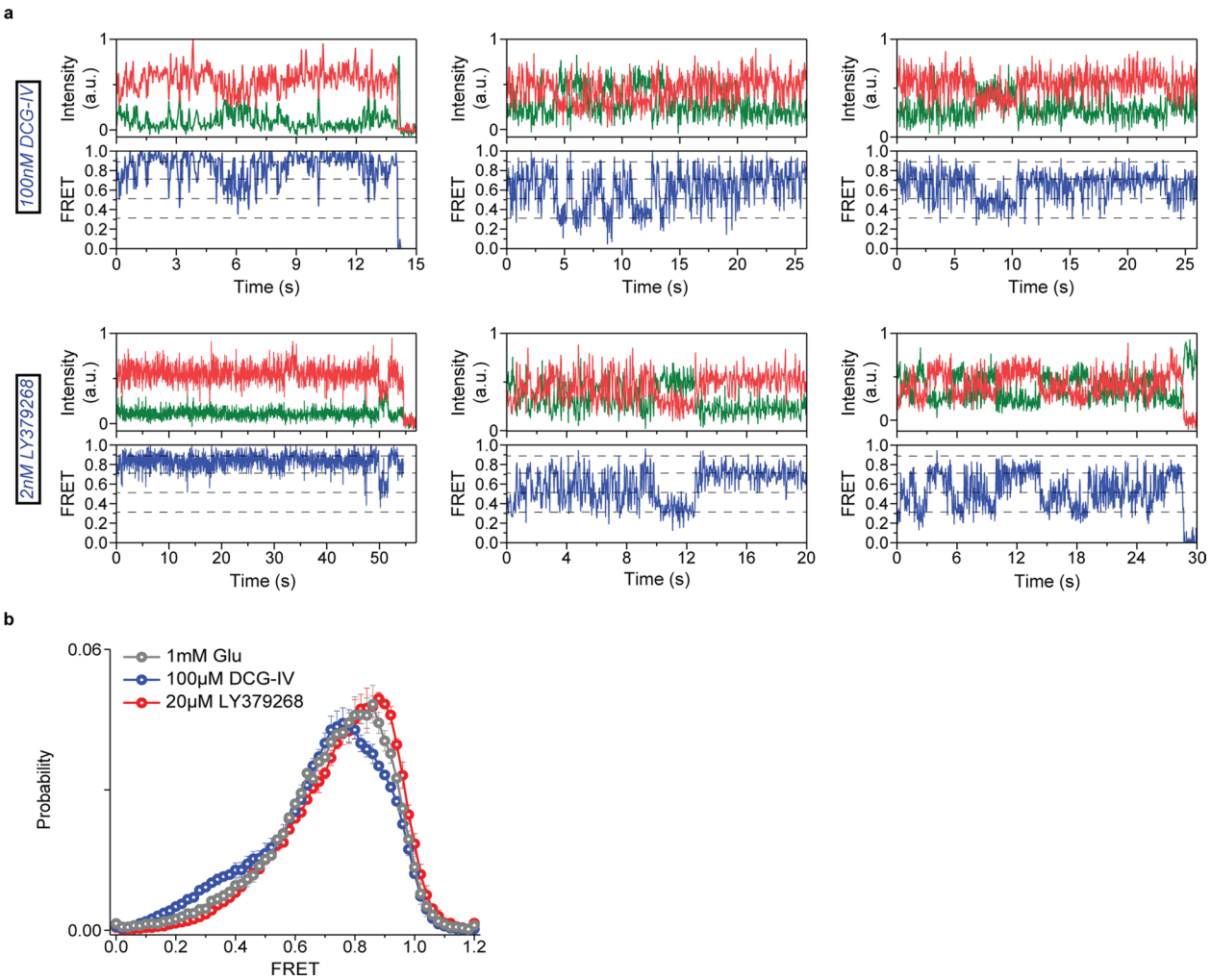

Extended Data Fig. 7 | smFRET analysis of CRD in the presence of orthosteric agonists. a, Example single-molecule time traces of 548UAA at intermediate concentrations of DCG-IV (100 nM, top) and LY379268 (2 nM, bottom) showing donor (green) and acceptor (red) intensities and corresponding FRET (blue). Dashed lines represent 4 distinct FRET states. **b**, smFRET population histograms for 548UAA in the presence of saturating glutamate (1 mM; 152 total molecules), DCG-IV (100 μM; 470 total molecules) and LY379268 (20 μM; 356 total molecules). Data represent mean ± s.e.m. of N=3 independent experiments.

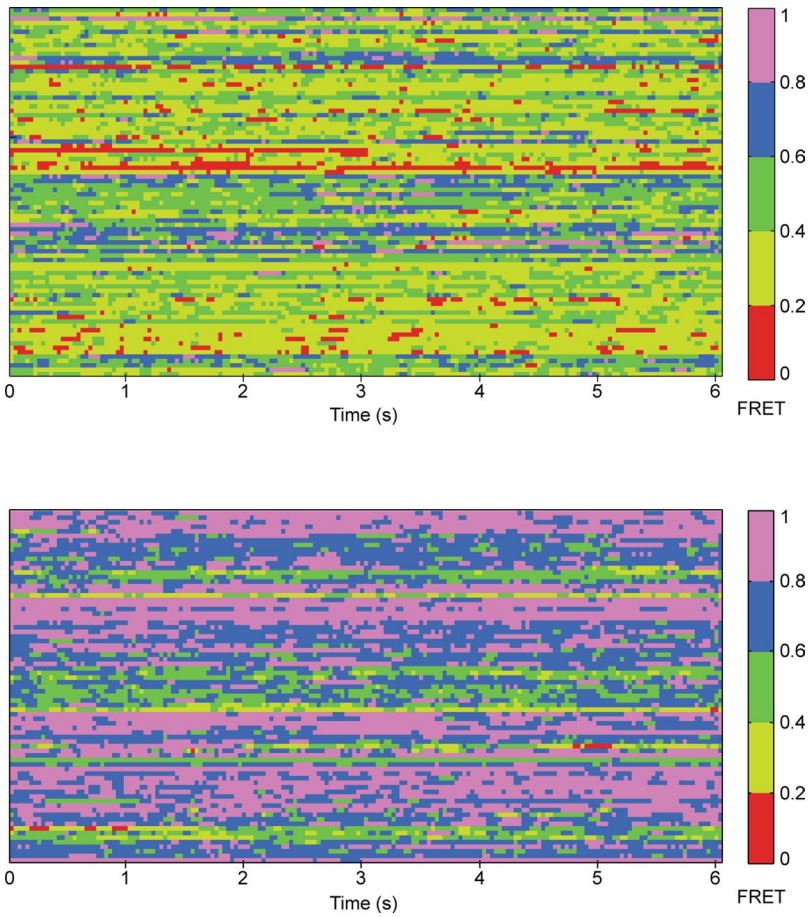

Extended Data Fig. 8 | CRDs of mGluR2 are dynamic. Heatmap illustrating the FRET values sampled by individual 548UAA receptors in the inactive (0 μM glutamate, top) and fully active (1 mM glutamate, bottom) conditions. Each row is the smFRET time trace of a single molecule over 6 seconds. The smFRET traces were smoothed using a 3-point moving average filter. 100 independent molecules are shown for each condition.

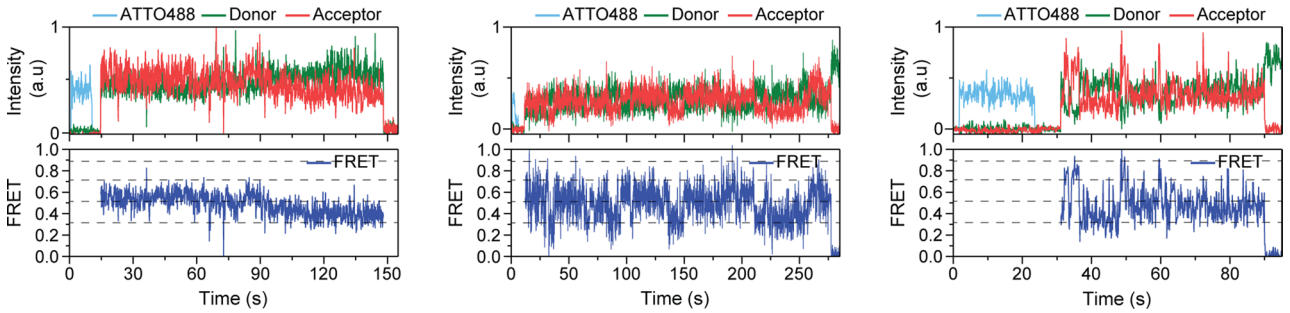

Extended Data Fig. 9 | Analysis of conformational state 2 and state 4. Example single-molecule time traces of 548UAA YADA/WT heterodimers at 20 μM glutamate. ATTO488 (light blue), donor (green) and acceptor (red) intensities and the corresponding FRET (blue) are shown. Dashed lines represent 4 distinct FRET states. Data was acquired at 100 ms time resolution.

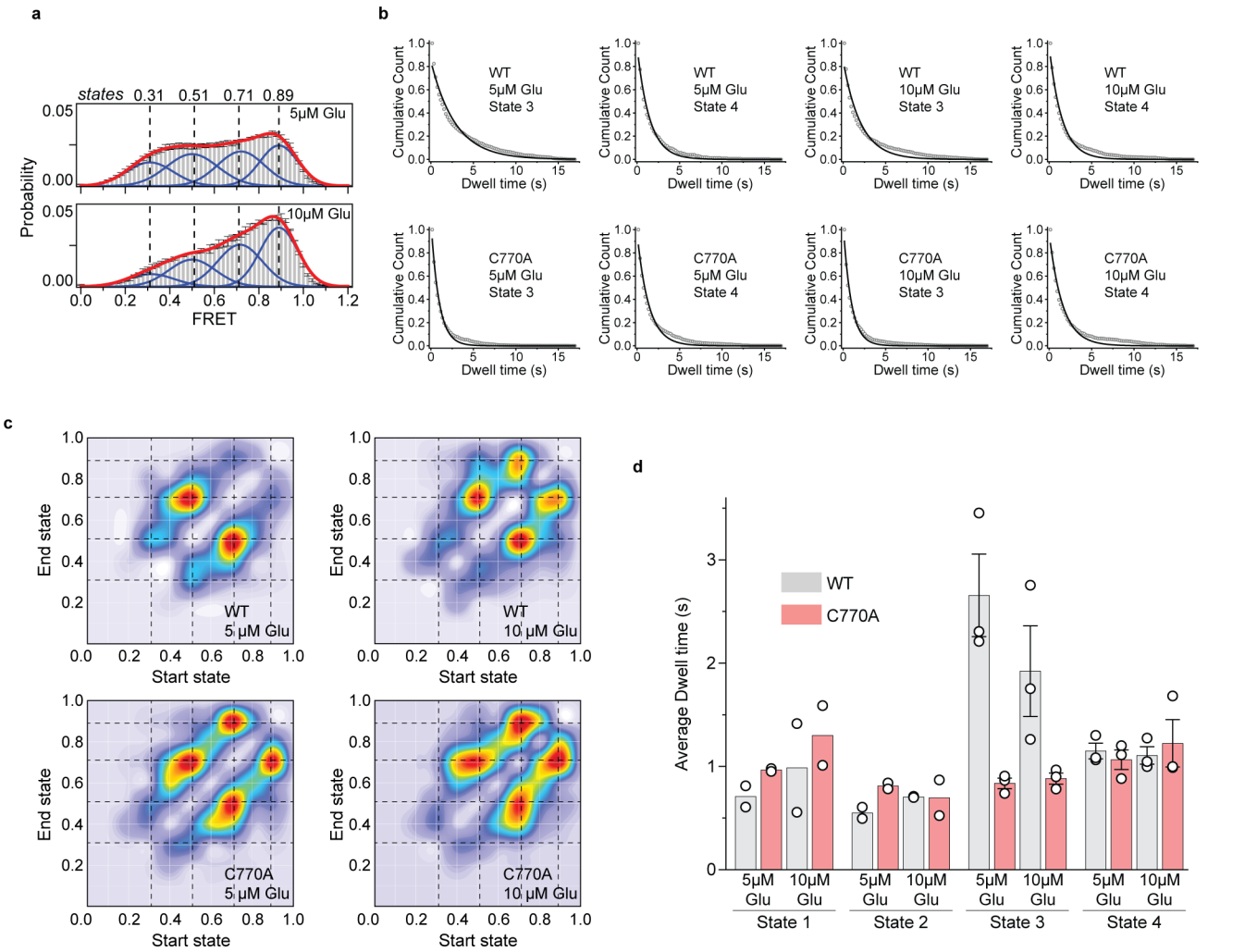

Extended Data Fig. 10 | Characterization of the mGluR2 PAM mutant conformational dynamics. a, smFRET population histograms of 548UAA PAM mutant (C770A) in the presence of 5 μM (689 total molecules) or 10 μM (370 total molecules) glutamate. Histograms are fitted (red) to 4 Gaussian distributions (blue) centered around 0.31 (state 1), 0.51 (state 2), 0.71 (state 3) and 0.89 (state 4), denoted with dashed lines. Data represent mean ± s.e.m. of N=3 independent experiments. **b**, Normalized histograms of state 3 (pre-active) and state 4 (active) dwell times (cumulative count) in the presence of 5 or 10 μM glutamate for 548UAA and 548UAA PAM mutant (C770A). Data is fit to a single exponential decay function. Dwell times are from > 80 total molecules per condition from two independent experiments. **c**, TDPs of 548UAA and 548UAA PAM mutant (C770A) at 5 or 10 μM glutamate. Dashed lines represent 4 distinct FRET states. Transitions are compiled from two independent experiments. **d**, Dwell times of states 1-4 for 548UAA and 548UAA PAM mutant (C770A) in the presence of 5 or 10 μM glutamate. Average dwell time was calculated by fitting a single exponential decay function to dwell-time histograms for each condition. Dwell times of states 1 and 2 represent the mean of N=2 independent experiments with 86, 83, 91 and 72 total molecules examined for WT (5 μM), WT (10 μM), C770A (5 μM) and C770A (10 μM), respectively. Dwell times of states 3 and 4 represent the mean ± s.e.m. of N=3 independent experiments with 147, 140, 128 and 142 total molecules examined for WT (5 μM), WT (10 μM), C770A (5 μM) and C770A (10 μM), respectively. Transition and dwell-time analysis were performed on 100 ms data.

nature research

Corresponding author(s): Reza Vafabakhsh

Last updated by author(s): Oct 14, 2020

Reporting Summary

Nature Research wishes to improve the reproducibility of the work that we publish. This form provides structure for consistency and transparency in reporting. For further information on Nature Research policies, see our Editorial Policies and the Editorial Policy Checklist.

Statistics

For all statistical analyses, confirm that the following items are present in the figure legend, table legend, main text, or Methods section.

n/a	Confirmed
☐	☒ The exact sample size (*n*) for each experimental group/condition, given as a discrete number and unit of measurement
☐	☒ A statement on whether measurements were taken from distinct samples or whether the same sample was measured repeatedly
☒	☐ The statistical test(s) used AND whether they are one- or two-sided *Only common tests should be described solely by name; describe more complex techniques in the Methods section.*
☒	☐ A description of all covariates tested
☒	☐ A description of any assumptions or corrections, such as tests of normality and adjustment for multiple comparisons
☐	☒ A full description of the statistical parameters including central tendency (e.g. means) or other basic estimates (e.g. regression coefficient) AND variation (e.g. standard deviation) or associated estimates of uncertainty (e.g. confidence intervals)
☒	☐ For null hypothesis testing, the test statistic (e.g. *F*, *t*, *r*) with confidence intervals, effect sizes, degrees of freedom and *P* value noted *Give P values as exact values whenever suitable.*
☒	☐ For Bayesian analysis, information on the choice of priors and Markov chain Monte Carlo settings
☒	☐ For hierarchical and complex designs, identification of the appropriate level for tests and full reporting of outcomes
☒	☐ Estimates of effect sizes (e.g. Cohen's *d*, Pearson's *r*), indicating how they were calculated

Our web collection on statistics for biologists contains articles on many of the points above.

Software and code

Policy information about availability of computer code

Data collection	Single-molecule and cell-based TIRF data acquisition were done using smCamera (version 1.0), which is previously published software and is available at (http://ha.med.jhmi.edu/resources/). Confocal image data acquisition was done using Zen (Blue Edition; 2.3 system).
Data analysis	Softwares used for analysis include: smCamera (version 1.0; http://ha.med.jhmi.edu/resources/), OriginPro 2018b (b 9.5.5.409), MATLAB 2013b (8.2.0.701), Chimera (1.13.1) and ImageJ (1.52P). vbFRET (version 2.5; last edited 10-7-2009) is an open source MATLAB package used to generate idealized traces for single-molecule data. The custom codes for data analysis are available from the corresponding author upon request.

For manuscripts utilizing custom algorithms or software that are central to the research but not yet described in published literature, software must be made available to editors and reviewers. We strongly encourage code deposition in a community repository (e.g. GitHub). See the Nature Research guidelines for submitting code & software for further information.

Data

Policy information about availability of data

All manuscripts must include a data availability statement. This statement should provide the following information, where applicable:

- Accession codes, unique identifiers, or web links for publicly available datasets
- A list of figures that have associated raw data
- A description of any restrictions on data availability

The materials and data reported in this study are available from the corresponding author upon reasonable request. The PDB accession code for the inactive and active structures of human mGluR5 are 6N52 and 6N51. Source data are provided with this paper.

Field-specific reporting

Please select the one below that is the best fit for your research. If you are not sure, read the appropriate sections before making your selection.

☒ Life sciences ☐ Behavioural & social sciences ☐ Ecological, evolutionary & environmental sciences

For a reference copy of the document with all sections, see nature.com/documents/nr-reporting-summary-flat.pdf

Life sciences study design

All studies must disclose on these points even when the disclosure is negative.

Sample size	No statistical method was used to predetermine sample sizes. Sample size of more than 1000 molecules per condition was acquired and was found to adequately sample the behavior of molecules. Increasing the number of molecules acquired did not change our results, suggesting that our sample size was sufficiently large. Standard replicate sizes of n=3+ was used. All the biological samples and reagents were made fresh for each experiment.
Data exclusions	Exclusion criteria to remove artifacts were described in detail in the manuscript, applied uniformly to all the samples, and were pre-established. For cell-based experiments, cells and ROIs showing substantial drift, lateral movement, and a lack of anti-correlated behavior of donor and acceptor signals were excluded. For idealized trace fitting to single-molecule data, occasional traces for which the HMM fit did not converge (for example due to long blinking events or large non anti-correlated intensity fluctuations) were omitted from downstream analysis.
Replication	All the experiments were repeated (with similar results) at least five times. No biological material was used in more than one set of experiments. In most cases data from 3 independent experiments were averaged in final figures.
Randomization	Randomization was not practical in this study. No significant bias in single-molecule and cell-based experiments have been observed due to physical or time constraints of our experimental setup and design.
Blinding	All data was analyzed by three individuals independently and the results were compared and showed to be identical. In addition, a subset of data was blindly analyzed to ensure no bias in analysis for different conditions for each individual.

Reporting for specific materials, systems and methods

We require information from authors about some types of materials, experimental systems and methods used in many studies. Here, indicate whether each material, system or method listed is relevant to your study. If you are not sure if a list item applies to your research, read the appropriate section before selecting a response.

Materials & experimental systems

n/a	Involved in the study
☐	☒ Antibodies
☐	☒ Eukaryotic cell lines
☒	☐ Palaeontology and archaeology
☒	☐ Animals and other organisms
☒	☐ Human research participants
☒	☐ Clinical data
☒	☐ Dual use research of concern

Methods

n/a	Involved in the study
☒	☐ ChIP-seq
☒	☐ Flow cytometry
☒	☐ MRI-based neuroimaging

Antibodies

Antibodies used	DYKDDDDK Tag Antibody [Biotin], Mouse. From GenScript Cat. No. A01429
Validation	Quality control tests for reactivity were performed by the manufacturer and showed an ELISA titer ≥1:20,000 and also passed western blot validation by showing specific reactivity for DYKDDDDK-tagged proteins. For our purposes the anti-FLAG antibody was

used for pull-down of receptors in the single-molecule FRET assay. Antibody did not pull-down fluorescently labeled receptors without the FLAG tag.

Eukaryotic cell lines

Policy information about cell lines

Cell line source(s)	HEK-293T cells were purchased from Millipore-Sigma for this study.
Authentication	Cell lines were not authenticated.
Mycoplasma contamination	Cell lines were not tested for mycoplasma contamination.
Commonly misidentified lines (See ICLAC register)	No commonly misidentified cell lines were used in the study.